ROYAL SOCIETY OF CHEMISTRY

NJC

Effects of *N,N*-heterocyclic ligands on the *in vitro* cytotoxicity and DNA interactions of copper(II) chloride complexes from amidino-*O*-methylurea ligands

SCHOLARONE™
Manuscripts

1

1　　**Manuscript_R2**

4　**Title** Effects of *N,N*-heterocyclic ligands on the *in vitro* cytotoxicity and DNA

5　interactions of copper(II) chloride complexes from amidino-*O*-methylurea ligands

6　**Authors** Atittaya Meenongwa,[a] Rosa F. Brissos,[b] Chaiyaporn Soikum,[c] Prapansak Chaveerach,[c]

7　Patrick Gamez,[bd] Yanee Trongpanich[e] and Unchulee Chaveerach[a,*]

8　*[a] Materials Chemistry Research Center, Department of Chemistry and Center of Excellence for*

9　*Innovation in Chemistry, Faculty of Science, Khon Kaen University, Khon Kaen 40002, Thailand*

10　*[b] Departament de Química Inorgànica, Universitat de Barcelona, Martí I Franqués 1-11, 08028*

11　*Barcelona, Spain*

12　*[c] Department of Veterinary Public Health, Faculty of Veterinary Medicine, Khon Kaen University,*

13　*Khon Kaen 40002, Thailand*

14　*[d] Institució Catalana de Recerca i Estudis Avançats (ICREA), Passeig Lluís Companys, 23, 08010*

15　*Barcelona, Spain*

16　*[e] Department of Biochemistry, Faculty of Science, Khon Kaen University, Khon Kaen 40002,*

17　*Thailand*

18

19

20

21

22

23

Abstract

Development of the biological activities of the copper(II) complexes based on guanidine derivatives have been carried out by addition of *N,N*-heterocyclic ligands, yielding the four new compounds, $[Cu(L^1)(bipy)]Cl_2$ (**1**), $[Cu(L^1)(phen)]Cl_2$ (**2**), $[Cu(L^2)(bipy)Cl_2]$ (**3**) and $[Cu(L^2)(phen)]Cl_2$ (**4**) (L^1 = amidino-*O*-methylurea, L^2 = *N*-(benzyl)-amidino-*O*-methylurea, bipy = 2,2-bipyridine and phen = 1,10-phenanthroline). All complexes were characterized by elemental analysis and various spectroscopic methods (FT-IR, mass, diffuse reflectance, UV-Vis and EPR). Their possible structures were proposed to be square planar (for **1**, **2** and **4**) and distorted octahedral structures (for **3**). Their interactions with calf thymus (CT) DNA were examined by electronic absorption titration, viscosity measurements, circular dichroism spectroscopy, DNA-melting analysis, fluorescence spectroscopy and determination of the stoichiometry. Two possible DNA-binding modes of the complexes are proposed to be non-intercalation at low [Complex]/[DNA] ratio and intercalation at high [Complex]/[DNA] ratio. Their nuclease activities investigated by gel-electrophoresis and atomic-force microscopy (AFM) show that the complexes can cleave the plasmid pBR322 DNA probably through oxidative pathway. Moreover, their *in vitro* cytotoxic activities against three human tumor cells (the small cell lung carcinoma (NCI-H187), the oral cavity carcinoma (KB) and the breast adenocarcinoma (MCF-7)) and their antibacterial activities toward three negative bacteria (*E. coli*, *Salmonella* and *Campylobacter*) were determined. The complexes in this system exhibit a more potent anticancer effect against the NCI-H187 cell line. Complex **2** gives the best inhibition efficiency, especially *Campylobacter*. Indeed, the biological activities of the complexes are in the trend of **2** > **4** > **1** > **3**.

1. Introduction

DNA interactions with inorganic compounds have been intensely investigated their mechanisms. The obtained valuable information is of paramount importance in developing the metal-based drugs. A square planar platinum complex $[Pt(NH_3)_2Cl_2]$ or cisplatin, the first generation anticancer drug,[1]

1   shows high cytotoxicity to several types of cancers such as testicular, ovarian, head and neck and cell

2   lung cancers[2] by coordination with DNA, leading to interfere with mitosis and then the cancer cell

3   undergoing apoptosis.[3] Nevertheless, several side-effects of cisplatin encourage many researchers for

4   developing new metal-based anticancer drugs with higher curative potential, lower toxicities and

5   target-specific properties.

6   Copper is recognized as a bio-essential trace element for human body due to the enzymatic

7   functions arising from its oxidative nature.[4] In addition, copper is cheaper and can give the

8   complexes with various coordination geometries. Some copper(II) complexes with organic ligands

9   are reported to be effective DNA-binding and cleaving agents as well as active against bacteria and

10   cancer cells.[5–7] Consequently, copper is suitable to be an alternative element providing the benefits in

11   both design and various applications.

12   In our previous works, a series of copper(II) complexes containing the bidentate amidino-*O*-

13   methylurea (L^1) and *N*-(benzyl)-amidino-*O*-methylurea (L^2) have been intensively investigated on

14   their biological behaviors. These ligand systems have versatile hydrogen-bonding potential[8,9] which

15   possibly involves in the biological activities of the copper(II) complexes. Two monomeric copper(II)

16   compounds, $[Cu(L^1)_2Cl_2]$ and $[Cu(L^2)_2Cl_2]$, with a square planar geometry[9] display the DNA-binding

17   capability through non-intercalative modes, the DNA-cleaving ability *via* oxidative process and the

18   antibacterial activity toward *Campylobacter*.[10] Recently, two dimeric compounds of these ligands,

19    $[Cu(L^1)Cl_2]_2$ and $[Cu(L^2)Cl_2]_2$, with the proposed structure as an approximate square-pyramidal

20   geometry[11] exhibit the DNA-binding and cleaving properties, antibacterial activity against three

21   human-food poisoning bacteria including *Salmonella*, *E. coli* and *Campylobacter* as well as

22   anticancer activity toward small cell lung carcinoma and epidermoid carcinoma of oral cavity.[12]

23   In this work, the biological properties of the copper(II) complexes based on the dimeric

24   compounds $[Cu(L^1)Cl_2]_2$ and $[Cu(L^2)Cl_2]_2$ have been improved by the addition of *N*,*N*-heterocyclic

25   ligands. 2,2′-Bipyridine (bipy) and 1,10-phenanthroline (phen) were selected as the second ligand.

1   Some copper(II) complexes containing bipy or phen have shown the DNA-binding and DNA

2   cleavage properties.[6,13–15] Herein, we report the synthesis and characterization of the four copper(II)

3   complexes including $[Cu(L^1)(bipy)]Cl_2$ (**1**), $[Cu(L^1)(phen)]Cl_2$ (**2**), $[Cu(L^2)(bipy)Cl_2]$ (**3**) and

4    $[Cu(L^2)(phen)]Cl_2$ (**4**). To investigate the potential DNA-binding properties of the complexes toward

5   calf thymus (CT) DNA, several methods including electronic absorption titration, viscosity

6   measurements, circular dichroism (CD) spectroscopy, thermal denaturation, fluorescence

7   spectroscopy and determination of stoichiometry were employed. The effective DNA cleavage of the

8   complexes was further examined by gel electrophoresis and atomic-force microscopy (AFM) toward

9   pBR322 plasmid DNA. Their cytotoxicity against three human cancer cell lines (*i.e.* small cell lung

10   carcinoma (NCI-H187), epidermoid carcinoma of the oral cavity (KB) and breast adenocarcinoma

11   (MCF-7)) was determined using the resazurin microplate assay (REMA). Furthermore, all complexes

12   were screened for their antibacterial activity against a series of human food-poisoning bacteria

13   (*Salmonella*, *E. coli* and *Campylobacter*) by the agar-well diffusion method.

14   **2.   Experimental**

15   **2.1. Materials and Instruments**

16   2,2′-Bipyridine (bipy) and 1,10-phenanthroline monohydrate (phen) were obtained from Acros

17   Organics and Carlo Erba, respectively. All other chemicals and solvents (analytical grade) were

18   commercially available and used without further purification. DNA sodium salt from calf thymus

19   (CT-DNA, Type I fibrous) was purchased from Sigma-Aldrich. Plasmid pBR322 DNA (4361 bp,

20   0.25 µg µL^{-1}) was obtained from Bio Basic INC and Roche Farma, S.A. Tris(hydroxymethyl)

21   aminomethane (Tris base) and ethidium bromide (EB) solution (10 mg mL^{-1}) were purchased from

22   Promega. Agarose (D-1, Low EEO) was purchased from Pronadisa. *N*-(2-Hydroxyethyl)piperazine-

23   *N′*-(2-ethanesulfonic acid) (HEPES) was obtained from Sigma-Aldrich. All reagents involving in the

24   DNA experiments were molecular biology grade and used as received. Doubly distilled water was

used to prepare the buffer solution (3% MeOH in Tris-buffer containing 5 mM Tris-HCl and 50 mM NaCl, pH = 7.2).

Elemental analyses (C, H and N) were determined using a Perkin-Elmer PE-2400II CHNS/O elemental analyzer. Infrared spectra were recorded in the range of 400–4000 cm^{-1} using KBr pellets on a Perkin-Elmer Spectrum One FT-IR spectrophotometer. Electrospray ionization (ESI+) mass spectra in MeOH were recorded on a Bruker micrOTOF mass spectrometer. Diffuse reflectance spectra were collected on a Shimadzu 3101 UV-Vis-NIR scanning spectrophotometer. Electronic absorption spectra of sample solutions in MeOH and DMSO were recorded on an Agilent 8453 UV-Vis spectrophotometer using cuvettes of 1 cm path length. Electron spin resonance spectra in the frozen DMSO solutions at 77 K were detected by a RE-2X electron spin resonance spectrometer operating at ν = 9.16 GHz (X-band). Fluorescence measurements were analyzed with a Shimadzu RF–5301PC spectrofluorophotometer. Circular dichroism (CD) spectra were recorded on a Jasco J-815 spectropolarimeter (the service was provided by Research Instrument Center, Khon Kaen University, Thailand). The amount of copper for each stoichiometric ratio was determined with a Perkin-Elmer AAnalyst 100 atomic absorption spectrophotometer. The electrophoretic band intensities were visualized with a Bio-Rad Gel Doc 2000 system using the LABWORK software. The atomic-force microscopy (AFM) images were obtained by a Nanoscope V Multimode 8 AFM (Bruker AXS) operating in the PEAK FORCE tapping mode. Commercial Si-tip on Nitride lever cantilevers (SNL, Bruker) with force constant of 0.4 N m^{-1} was used.

2.2. Complex preparation

2.2.1. Copper(II) complexes of amidino-*O*-methylurea and its derivative. The two dimeric copper(II) complexes, [Cu(L^1)Cl$_2$]$_2$ and [Cu(L^2)Cl$_2$]$_2$ were prepared according to our published procedure[16] and used as the starting complexes.

1   **2.2.2. Copper(II) complexes with *N,N*-heterocyclic ligands.** A methanolic solution (25 mL)

2   of 2,2′-bipyridine (0.1562 g, 1 mmol) or 1,10-phenanthroline monohydrate (0.1980 g, 1 mmol) was

3   added dropwise to a methanolic solution (25 mL) of $[Cu(L^1)Cl_2]_2$ (0.2505 g, 0.5 mmol) or

4    $[Cu(L^2)Cl_2]_2$ (0.3405 g, 0.5 mmol) under stirring at ambient temperature, and subsequently adjusted

5   pH to 7 by NaOH. The reaction mixture was stirred for 2 h and filtered off. The volume of the filtrate

6   was reduced by 50% and left for slow evaporation. The purple or pink product was achieved and

7   further recrystallized in ethanol.

8   *[Cu(L^1)(bipy)]Cl$_2$ (1)*: Purple solid. Yield, 0.3486 g, 85.8%. Anal. Calc. for $C_{13}H_{16}CuN_6OCl_2$

9   (MW. 406.50) (%): C, 38.38; H, 3.94; N, 20.66. Found: C, 37.69; H, 4.04; N, 20.63. Melting point

10   (°C): 127.5−128.4. FT-IR (KBr, cm^{-1}): 3429s, 3323s, 1613m, 1583s, 1528m, 1498m, 1474m, 1448m,

11   1405m, 1317w, 1282w, 1223w, 1193w, 1137w, 1095w, 1071w, 1032w, 1019w, 966w, 771w, 729w,

12   683w, 635w, 534w, 414w. Solubility: High soluble in polar solvents such as water, MeOH and

13   DMSO.

14   *[Cu(L^1)(phen)]Cl$_2$ (2)*: Purple solid. Yield, 0.3136 g, 72.8%. Anal. Calc. for $C_{15}H_{16}CuN_6OCl_2$

15   (MW. 430.7) (%): C, 41.79; H, 3.71; N, 19.50. Found: C, 41.45; H, 3.91; N, 19.39. Melting point

16   (°C): 171.7−172.3. FT-IR (KBr, cm^{-1}): 3486s, 3394s, 3322s, 3208s, 3060m, 1643s, 1574s, 1523s,

17   1494s, 1469s, 1428m, 1393m, 1347w, 1289w, 1224m, 1190m, 1149w, 1099m, 1007w, 927w, 872w,

18   851m, 780w, 735w, 722m, 645w, 574w, 521w. Solubility: High soluble in polar solvents such as

19   water, MeOH and DMSO.

20   *[Cu(L^2)(bipy)Cl$_2$](3)*: Pink solid. Yield, 0.1876 g, 37.8%. Anal. Calc. for $C_{20}H_{22}CuN_6OCl_2$

21   (MW. 496.5) (%): C, 48.32; H, 4.43; N, 16.91. Found: C, 48.44; H, 4.59; N, 17.06. Melting point

22   (°C): 180.0−181.3. FT-IR (KBr, cm^{-1}): 3369m, 3332m, 2951w, 2923w, 1589s, 1495s, 1472s, 1451s,

23   1414s, 1394s, 1357m, 1323w, 1262m, 1219w, 1199w, 1189w, 1122w, 1090w, 1067w, 1026w,

24   1001w, 934w, 756m, 708m, 594w, 580w. Solubility: High soluble in MeOH and DMSO but

25   insoluble in water.

1    $[Cu(L^2)(phen)]Cl_2$ *(4)*: Purple solid. Yield, 0.4384 g, 84.2%. Anal. Calc. for $C_{22}H_{22}CuN_6OCl_2$

2   (MW. 520.7) (%): C, 50.70; H, 4.23; N, 16.13. Found: C, 50.79; H, 4.14; N, 15.65. Melting point

3   (°C): 189.0–190.4. FT-IR (KBr, cm^{-1}): 3434m, 3265m, 3123w, 3062w, 1605s, 1524s, 1495m, 1473s,

4   1427m, 1347w, 1277w, 1250w, 1221w, 1200w, 1186w, 1141w, 1126w, 1090w, 1042w, 928w, 906w,

5   853w, 758w, 719m, 580w. Solubility: High soluble in MeOH and DMSO but insoluble in water.

6   **2.3. DNA binding experiments**

7   To circumvent some problems caused by the organic solvents, Tris-buffer (5 mM Tris-HCl/50 mM

8   NaCl, pH = 7.2) containing 3% MeOH was selected for utilizing in all experiments of CT-DNA and

9   copper(II) complexes. The DNA stock solution prepared in this buffer gave a UV-absorbance ratio

10   A_{260}/A_{280} of about 1.8–1.9 (where A_{260} and A_{280} are the absorbances of a DNA sample at 260 and 280

11   nm, respectively), indicating that DNA was sufficiently free of protein contamination.[17] The stock

12   solution was kept at 4 °C and used within 4 days. A 10-fold dilution of DNA concentration was

13   determined spectrophotometrically at 260 nm by using the molar extinction coefficient value of 6600

14   M^{-1} cm^{-1}.[18] The stock solutions of both DNA and the copper(II) complexes were freshly prepared

15   before uses.

16   **2.3.1. Electronic absorption titration.** Absorption titration experiments were carried out with

17   a constant concentration of copper(II) complexes, *viz.* 10 μM, and varying the concentration of CT-

18   DNA (2–15 μM) in 3% MeOH/Tris-buffer at pH 7.2. The complex and DNA solutions were

19   incubated at 37 °C for 24 h. Subsequently, the spectra were recorded with a UV-Vis

20   spectrophotometer at ambient temperature. To subtract the absorption due to DNA itself (in each

21   sample), spectra of free CT-DNA (namely in the absence of copper compounds) were recorded at the

22   same concentrations of 2–15 μM, and were used as blanks. To compare the DNA-binding strength of

23   the four compounds, their intrinsic binding constant (K_b) was calculated from the plots of [DNA]/(ε_a

24   − ε_f) *vs.* [DNA] using Eq. (1); K_b is given by the ratio of the slope to the *y* intercept.[19]

$$[DNA]/(\varepsilon_a - \varepsilon_f) = [DNA]/(\varepsilon_b - \varepsilon_f) + 1/K_b(\varepsilon_b - \varepsilon_f) \tag{1}$$

Where [DNA] is the concentration of DNA, ε_a is given by $A_{obsd}/[Cu]$, ε_f is the extinction coefficient for the free metal complex and ε_b is the extinction coefficient for the metal complex in the fully bound form.

2.3.2. Viscometric titration. Viscosity experiments were carried out with an Ubbelodhe viscometer, immersed in a water bath at 37±0.1 °C. The viscosity of a 200 µM solution of CT-DNA was determined in the presence of the complexes using different [Complex]/[DNA] ratios in the range of 0.00−2.00 with 0.20 intervals. The flow time for each sample was recorded in triplicate with a digital stopwatch, and then averaged. The relative viscosity (η) was determined from the flow time of the DNA-containing solutions (t) corrected by the flow time of the free buffer (t_0): $\eta = (t-t_0)/t_0$.[20] The data are presented as the plot of the relative viscosity, *i.e.* $(\eta/\eta_0)^{1/3}$, *vs.* [Complex]/[DNA]. η_0 and η are the viscosity of the free DNA solution and the DNA-complex solution, respectively.

2.3.3. Circular dichroism (CD) spectroscopy. Solutions of CT-DNA (200 µM) with the [Complex]/[DNA] ratios of 0.0, 0.5 and 1.0 were incubated at 37 °C for 24 h. The CD spectra of these solutions were recorded from 200 to 400 nm using a quartz cuvette with an optical path length of 10 mm and a scanning rate of 100 nm min^{-1}. The data were collected in triplicate with a time constant of 1 sec and a spectral bandwidth of 1.0 nm. The background signal due to the buffer was subtracted.

2.3.4. DNA-melting analysis. The DNA denaturation experiments in the presence of the copper(II) complexes with the [Complex]/[DNA] ratios of 0.5, 1.0, 1.5 and 2.0 were performed by monitoring the variation of the absorption intensity of DNA (200 µM) at 259 nm when the temperature of DNA solution was increased from 25.0 to 100.0 °C. All data were collected at each 5 °C and presented as the normalized absorbance, $(A - A_0)/(A_f - A_0)$, versus temperature, where A_f, A_0, and A are the final, the initial, and the observed absorbance at 259 nm, respectively. The melting

1   temperature (T_m) was determined from the maximum of the first derivative curve or tangentially from

2   the graph at the midpoint of the transition curve. ΔT_m was defined as the difference between T_m of the

3   free DNA and T_m of the bound DNA.

4   **2.3.5. Fluorescence spectroscopy.** Emission intensity measurements of ethidium bromide

5   (EB) with free CT-DNA in the absence and presence of complexes **1-4** were performed in 3%

6   MeOH/Tris-buffer, pH = 7.2. The CT-DNA solution (50 µM) was pretreated with EB (25 µM) for 30

7   min at room temperature and stored in the dark. The complex solution was then prepared (from the

8   previous stock solution of EB-DNA) in the [Complex]/[DNA] ratios of 0.0–1.0 with 0.1 intervals.

9   These solutions were kept in the dark for 30 min before measurement. The emission intensities

10   (between 550 and 700 nm) were obtained through the excitation at 500 nm.

11   To examine the fluorescence quenching mechanism, the Stern-Volmer quenching constant (K_{SV})

12   was determined by Eq. (2).[21]

$$F_0/F = 1 + K_{SV}[Q] \tag{2}$$

14   Where F_0 and F are the fluorescence intensities of the DNA-EB complex in the absence and presence

15   of copper(II) complexes, respectively. [Q] is the concentration of the complexes.

16   **2.3.6. Determination of stoichiometry of complex-DNA interactions.** The copper(II)/

17   DNA complex stoichiometry was determined by the similar procedure as described in the

18   literature.[22] The complex solution (3 mM, 1 mL) was added to the CT-DNA solution (*ca*. 3 mM,

19   1 mL), and the resulting mixture was incubated at 37 °C for 24 h. Precipitation of the DNA-

20   copper(II) complex was achieved by adding absolute ethanol (4 mL), NaCl (2 mM, 0.2 mL) and

21   keeping at −70 °C for 1 h. The precipitate was subsequently isolated by centrifugation at 4 °C (10000

22   rpm, 30 min). The supernatant was separated by pouring it out slowly. Next, deionized water (25 mL)

23   was added to dissolve the copper(II)/DNA precipitate. DNA concentration in the obtained DNA-

24   copper(II) complex solution was calculated (from triplicate experiments) by the absorption intensity

1 at 259 nm using $\varepsilon = 6600$ M^{-1} cm^{-1}.[18] The amount of copper(II) was determined by atomic

2 absorption spectroscopy, hence providing the Cu (mmol)/DNA (mol base) ratio.

2.4. DNA cleavage studies

4 **2.4.1. Gel electrophoresis.** Electrophoresis experiments were performed using the supercoiled

5 plasmid pBR322 DNA. The cleavage reactions of the plasmid DNA (0.2 µg, ~30 µM) were

6 undertaken in two conditions: (i) the addition of **1-4** alone (200, 400, 600 and 800 µM) and (ii) the

7 addition of **1-4** (10−400 µM for **1** and **3**; 0.1−4.0 µM for **2** and **4**) in the presence of ascorbic acid,

8 H$_2$ASC (100 µM). The total volume of all samples was adjusted to 10 µL by adding HEPES-buffer

9 (40 mM HEPES and 10 mM MgCl$_2$, pH = 7.2). The samples were incubated at 37 °C for 1 h.

10 Subsequently, a loading buffer (2 µL) containing 0.25% bromophenol blue, 0.25% xylene cyanol and

11 30% glycerol was added into the samples. The resulting mixtures were loaded into 0.8% agarose gel

12 and the fragment of each DNA form was separated by electrophoresis (50 V for 1.5 h in 1X TAE

13 buffer containing 40 mM Tris-acetate and 1 mM EDTA). The gel was stained with ethidium bromide

14 for 5 min and photographed under UV light. The proportion of the DNA forms was estimated by the

15 volume of the visualized DNA bands (volume = intensity × area) and used to determine the extent of

16 DNA cleavage. The intensities of the supercoiled DNA (Form I) were corrected by multiplying with

17 the factor value of 1.22 (for pBR322 DNA) because the intercalation between EB and Form I is

18 relatively weak when compared to that of nicked (Form II) and linear (Form III) DNA.[23] The extent

19 of DNA cleavage activity was calculated by the following Eq. (3).[24]

20 %DNA cleavage activity = {[volume of DNA-Form I)$_{control}$ − (volume of DNA-Form I)$_{sample}$]/

21 [volume of DNA-Form I)$_{control}$} × 100   (3)

22 **2.4.2. Atomic-force microscopy (AFM).** Plasmid pBR322 DNA (0.2 µg), heated at 60 °C for

23 15 min to open the supercoiled DNA, was incubated with the copper(II) complexes (400 µM for **1**

24 and **3**; 4.0 µM for **2** and **4**) in the presence of H$_2$ASC (100 µM) in 20 µL HEPES-buffer at 37 °C for

1　　1 h. Milli-Q water and all solutions for the AFM studies were filtered through 0.2 μm FP030/3 filters

2　　(Scheicher and Schuell GmbH, Germany) to obtain clear AFM images. After incubation, a drop (8

3　　μL) of each sample was placed onto peeled mica disks (PELCO Mica Discs, 9.9 mm diameter; Ted

4　　Pella, Inc. California, USA) and allowed to adsorb for 2 min at room temperature. The samples were

5　　rinsed for 5 sec with a stream of Milli-Q water directly onto the surface, which was subsequently

6　　blown dried with compressed argon before imaging.

7　　**2.5. Cytotoxicity assay**

8　　Cancer-cell growth inhibition of the copper(II) complexes against three human cancer cell lines

9　　namely the KB (epidermoid carcinoma of oral cavity, ATCC CCL-17), MCF-7 (breast

10　　adenocarcinoma, ATCC HTB-22) and NCI-H187 (small cell lung carcinoma, ATCC CRL-5804) cell

11　　lines was determined using Resazurin Microplate assay (REMA) as previously described method.[25]

12　　Ellipticine, doxorubicin and tamoxifen were used as positive controls, and 0.5% DMSO was used as

13　　a negative control. To investigate the potential cytotoxic behaviors of the copper(II) complexes, cells

14　　at a logarithmic growth phase were harvested and diluted in fresh medium to 7×10^4 cells mL^{-1} for

15　　KB, 9×10^4 cells mL^{-1} for MCF-7 and NCI-H187. Successively, 5 μL of the test sample diluted in 5%

16　　DMSO, and 45 μL of cell suspension were added to 384-well plates and then incubated at 37 °C in

17　　5% CO$_2$ incubator. After the incubation period (3 days for KB and MCF-7, and 5 days for NCI-

18　　H187), 12.5 μL of 62.5 μg mL^{-1} resazurin solution was added to each well, and the plates were then

19　　incubated at 37 °C for 4 h. Fluorescence signal was measured using SpectraMax M5 multi-detection

20　　microplate reader (Molecular devices, USA) at the excitation and emission wavelengths of 530 nm

21　　and 590 nm, respectively. Percentage inhibition of the cell growth was calculated by Eq. (4).

22　　$$\% \text{ Inhibition} = [1 \times (FU_T/FU_C)] \times 100 \tag{4}$$

23　　Where FU_T and FU_C are the mean fluorescence unit from the treated and untreated conditions by the

24　　copper(II) complexes, respectively. The anticancer activity of the complexes was expressed as 50%

1   inhibitory concentration (IC$_{50}$) determined from dose-response curves using the SOFTMax Pro

2   software (Molecular devices, USA). The plotted data were obtained from 6 concentrations of 2 fold

3   serially diluted test samples. The complexes with IC$_{50}$ > 50 µg mL^{-1} were considered to be inactive.[26]

4   **2.6. Antibacterial activity studies**

5   The screening of the *in vitro* antibacterial activity of the copper(II) complexes (50 mg mL^{-1}) against

6   three Gram-negative bacteria (*Salmonella*, *E. coli* and *Campylobacter*) was performed by the agar-

7   well diffusion method.[27] Active culture of the bacteria was transferred into 0.75% (w/w) semisolid

8   brucella agar (10 mL) at 50 °C. Subsequently, the incubated medium was swirled to distribute the

9   cell culture of bacteria and held at room temperature for 30 min. A well of 6 mm diameters was made

10   aseptically. The plates were placed at 37 °C for 48 h under the appropriate conditions to allow the

11   cell culture growth. Each complex was dissolved in 3% MeOH/Tris-buffer, pH = 7.2 to give the final

12   concentration of 1000 µg mL^{-1} and transferred into a well aseptically. The inhibitory activity of the

13   complex on bacteria was obtained from a clearing zone around the disc. The minimum inhibitory

14   concentration (MIC) values were also determined by two-fold serial dilution method in liquid media

15   containing the tested complexes.[28] The experiments were carried out in duplicate.

16   **3. Results and discussion**

17   **3.1. Complex preparation**

18   **3.1.1. General chemistry.** Our previous study reported the interesting biological properties and

19   cytotoxicity of the copper(II) chloride complexes containing 1-amidino-*O*-methylurea (L^1) and *N*-

20   (benzyl)-amidino-*O*-methylurea (L^2), [Cu(L^1)Cl$_2$]$_2$ and [Cu(L^2)Cl$_2$]$_2$.[16] Such a behaviour led us to

21   further investigate those two copper(II) compounds with one more ligand to improve their activities.

22   *N,N*-Heterocyclic ligands which are 2,2′-bipyridine (bipy) and 1,10-phenanthroline (phen) were

23   selected in order to their planar geometries and various beneficial biological activities (*e.g.* antitumor,

1   antifungal, antiviral and antimycoplasmal activities).[29–32] Herein, four new complexes **1-4** were

2   prepared by the reaction of the blue dimeric complexes $[Cu(L^1)Cl_2]_2$ or $[Cu(L^2)Cl_2]_2$ with bipy or

3   phen in a 1:2 molar ratio at pH 7 in MeOH.

4   The colors of all four products were changed from blue to purple for **1**, **2** and **4** and pink for **3**,

5   indicating that the environment around their copper(II) centers differs from those of the starting

6   compounds. This modification is the first evidence to point that the reactions have been taken place.

7   To gain more information to confirm the formation of **1**, **2**, **3** and **4**, various techniques were utilized

8   including infrared spectroscopy, elemental analysis, mass spectrometry, diffuse reflectance, UV-Vis

9   and electron paramagnetic resonance (EPR) spectroscopies.

10   Infrared spectra of the complexes **1-4** (Fig. 1) exhibit the characteristic bands of both chelating

11 *N,N*-heterocyclic ligands and the corresponding starting complexes. Strong and broad splitting bands

12 at $3486–3208 \text{ cm}^{-1}$ are assigned to the N–H stretching vibrations of the ligands L^1 and L^2.[16] The N–H

13 bending vibrations are shifted from $1692–1656 \text{ cm}^{-1}$ to lower frequencies at $1643–1589 \text{ cm}^{-1}$ upon

14 the coordination of the heterocyclic ligands. This situation has been found in our previous report.[16]

15 Such behavior indicates the existence of the ligands L^1 and L^2 in the products. Upon chelating of bipy

16 and phen, the ring stretching vibrations of C=C and C=N functional groups of free bipy (1578–1415

17 cm^{-1}) and phen ($1503–1421 \text{ cm}^{-1}$) are found to be shifted to higher frequencies at $1583–1448 \text{ cm}^{-1}$

18 for **1** and $1589–1451 \text{ cm}^{-1}$ for **3** (Fig. 1a) as well as at $1523–1428 \text{ cm}^{-1}$ for **2** and $1524–1427 \text{ cm}^{-1}$

19 for **4** (Fig. 1b). Additionally, the characteristic out-of-plane bending modes of free bipy (755–740

20 cm^{-1}) are shifted to 771 cm^{-1} for **1** and $756–708 \text{ cm}^{-1}$ for **3** while those of free phen ($853–738 \text{ cm}^{-1}$)

21 are shifted to $851–722 \text{ cm}^{-1}$ for **2** and $843–719 \text{ cm}^{-1}$ for **4**. Moreover, peaks assigned to the C–H

22 bending vibration of the phenyl ring on sidearm of the L^2 ligand at $1385–1226 \text{ cm}^{-1}$ were also

23 presented at $1394–1250 \text{ cm}^{-1}$. The changes in their vibrational energies of the functional groups upon

24 the complexation indicate the coordination of the two heterocyclic nitrogen donor atoms of bipy and

25 phen[33] with the copper center of the starting complexes.

2   **3.1.2. Prediction of chemical formula of the copper(II) complexes.** Data from elemental

3 analysis express the percentage of carbon, hydrogen and nitrogen of all four products in good

4 agreement with the chemical formulae of the desired copper(II) complexes which are

5 $[Cu(L^1)(bipy)]Cl_2$ (**1**), $[Cu(L^1)(phen)]Cl_2$ (**2**), $[Cu(L^2)(bipy)Cl_2]$ (**3**) and $[Cu(L^2)(phen)]Cl_2$ (**4**).

6   Additionally, the compositions of the products were interpreted from ESI+ mass spectra (Fig.

7 S1-S4). The ion peaks are listed in Table 1. The relative molecular ion peaks *i.e.* $[Cu(L^1)(bipy)]^{2+}$

8 ($m/z = 335$) for **1**; $[Cu(L^1)(phen)]^{2+}$ ($m/z = 359$) for **2**; $[Cu(L^2)(bipy)Cl_2+2H]^{2+}$ ($m/z = 497$) for **3**; and

9 $[Cu(L^2)(phen)]^{2+}$ ($m/z = 449$) for **4** were observed. Besides, the molecular fragment ions related to the

10 ligands and the relative abundance isotopes of ^{63}Cu and ^{65}Cu were also found in their spectra. Hence,

11 the obtaining evidence points us to ensure that four new copper(II) compounds have been achieved.

12 Furthermore, the ion species of copper-bipy or copper-phen complexes which were shown in the

13 spectra were probably formed in the ionization process during analysis.[34–37]

14   **"Table 1 Should be inserted here"**

15   **3.1.3. Prediction of the possible geometry of the copper(II) complexes.** With several

16 attempts, suitable single crystals of the complexes in this system were not achieved. Hence,

17 electronic absorption and X-band EPR spectroscopic methods were utilized to predict their

18 coordination geometries.

19   **3.1.3.1. Electronic absorption spectra.** Absorption spectra in solid and solution phases

20 of **1-4** were recorded (Fig. S5 and Table 2). In the solid state, the spectra of the purple complexes (**1**,

21 **2** and **4**) are similar and exhibit a strong band in the visible region at 526–567 nm (19 029–17 643

22 cm^{-1}) (Fig. S5a, b and d). While the spectrum of the pink complex **3** has a difference and shows two

23 overlapping absorption bands at 492 nm (20 300 cm^{-1}) and 560 nm (17 643 cm^{-1}) (Fig. S5c). In

24 addition, the spectra of **1-4** are compared with those of the square pyramidal starting compounds

1   ($[Cu(L^1)Cl_2]_2$ and $[Cu(L^2)Cl_2]_2$) which appear in blue with the d-d transition bands at 618−665 nm

2   (16 175−15 049 cm^{-1}).[11,16] The changes in color from blue for the starting compounds to purple or

3   pink for **1-4** together with a considerable blue shift preliminary suggest that the four complexes

4   reveal different coordination geometries and environments surrounding the copper(II) center from the

5   initial compounds. According to the results, the electronic absorption of **1**, **2** and **4** may be attributed

6   to a square planar geometry with the CuN_4 chromophore[38−40] which may arise from the chloride

7   replacement in $[Cu(L^1)Cl_2]_2$ and $[Cu(L^2)Cl_2]_2$ by two nitrogen donor atoms of the heterocyclic

8   molecule resulting in the shift to shorter wavelength of the d-d absorption bands of 139 nm (for **1**),

9   132 nm (for **2**) and 51 nm (for **4**). Whereas, the electronic spectrum of complex **3** informs that its

10 possible molecular geometry may adopt a distorted octahedron.[39,41] The further evidence to support

11 the proposed geometry of **3** is the electronic spectra of the distorted octahedral copper(II) complexes

12 of ethylenediamine and derivatives with the same CuN_4Cl_2 chromophore which exhibit a broad band

13 at 520−532 nm (19 200−18 800 cm^{-1}) with a shoulder at 581−585 nm (17 200−17 100 cm^{-1}),[41,42]

14 similar to the absorption of **3**.

15   **"Table 2 Should be inserted here"**

16   Moreover, it is essential to investigate the effect of solvents on the structures of the complexes

17 **1-4** to further confirm their possible geometries. It is due to the poor water solubility of **3** and **4**, the

18 electronic absorption spectra of all complexes were recorded in MeOH and DMSO. The color

19 changes of **1**, **2** and **4** from purple in solid state to purplish blue in MeOH and green in DMSO cause

20 to the shift of the absorption bands (Table 2). Such a result suggests that their coordination

21 geometries in solid state differ from those in solution phase due to the solvation effect. This may lead

22 us to ensure that **1**, **2** and **4** in the solid state are highly possible to adopt a square planar geometry

23 containing the vacant sites at the axial positions available for solvents. In the case of **3**, its spectra in

24 solid and in both organic solvents show somewhat alteration. However, the pink color of both phases

1   apparently remains unchanged, assuming that the solvent molecules do not interact with the

2   copper(II) center. Such a behavior may strengthen the coordination geometry of **3** as a distorted

3   octahedron.

4   **3.1.3.2. EPR spectra.** X-band EPR spectra provide alternative information to further

5   confirm the stereochemistry of the copper(II) complexes. All complexes exhibit anisotropic spectra

6   with the hyperfine splitting lines around the $g_{\parallel}$ region due to the interaction of the $S = 1/2$ electron

7   spin with the $I = 3/2$ copper nucleus (Fig. 2). The spin Hamiltonian parameters, g tensors values

8   describing the electronic ground state of the copper center show $g_{\parallel} > g_{\perp} > 2.0$ which are indicative of

9   a $d_{x^2-y^2}$ ground state corresponding to elongated tetragonal octahedral or square planar geometries

10   (Table 2).[43] Obviously, the distinction between the components of the $g_{\parallel}$ peak is difficult because of

11   the overlap with the $g_{\perp}$ peaks. Moreover, minor signals between the $g_{\parallel}$ components are found in the

12   spectra of **1**, **2** and **4**. This may be due to the interactions between the complexes and the solvent

13   molecules as likely observed in our previous report.[16] The parallel hyperfine coupling constant ($A_{\parallel}$) in

14   the range of 201-207 G supports a square-planar CuN_4 geometry in the complexes **1**, **2** and **4**[40] while

15   that of **3** ($A_{\parallel} = 216$ G) showing larger value together with lower $g_{\parallel}$ value is a characteristic of the

16   tetragonally elongated pseudooctahedral copper(II) complexes.[44,45] In comparison with the starting

17   compounds, changes in the spin Hamiltonian parameters (a decrease in $g_{\parallel}$ and an increase in $A_{\parallel}$

18   values) are observed since the two chloride ligands in $[Cu(L^1)Cl_2]_2$ or $[Cu(L^2)Cl_2]_2$ are replaced by

19   two nitrogen donors of the *N,N*-heterocyclic ligands yielding CuN_4 based complexes. Similarly, such

20   a behavior has been found in our previous works.[16] Moreover, a typical of superhyperfine interaction

21   of unpaired electron of the copper ion with four magnetically ^{14}N nuclease ($I = 1$) is found in their

22   spectra at the $g_{\perp}$ region with the superhyperfine coupling values (A_N) of 15 to 18 G (Table 2). These

23   parameters are close to those observed for the copper(II) ion coordinated in the equatorial plane by

24   four strong nitrogen donors provided by chelating   ligands.[16,46,47] On the other hand, this coupling is

25   unobservable in the starting complexes $[Cu(L^1)Cl_2]_2$ and $[Cu(L^2)Cl_2]_2$ (Fig. 2).

1   **"Fig. 2. Should be inserted here"**

2   The electronic absorption spectra and the spin Hamiltonian parameters derived from the

3   experimental EPR spectra allow us to identify the possible geometries of the copper(II) complexes

4   (Fig. 3). The proposed structures of **1**, **2** and **4** may adopt a similar geometry as a square planar with

5   four nitrogen donor atoms from the ligand L^1 or L^2 and the heterocycles (bipy or phen) yielding a

6   CuN_4 coordination sphere. In contrast, the different coordination structural arrangement is found for

7   **3** which possibly adopt a CuN_4Cl_2 octahedral geometry. The predicted coordination geometry of all

8   complexes may provide a better understanding in some properties related to their biological

9   activities.

10   **"Fig. 3. Should be inserted here"**

11   **3.2. DNA-binding studies of the complexes 1-4**

12   An essential property leading to the biological applications of the complexes is their DNA-binding

13   behaviors. In principle, the binding interactions are classified into two modes, covalent and non-

14   covalent. The former mode has found in cisplatin, a well known covalent DNA-binder which

15   interacts with DNA through coordinate covalent bonds at N7 guanine on the DNA strand.[3] There are

16   three major ways for the later mode; (i) intercalative binding between two adjacent base pairs and

17   perpendicular to the helical axis, (ii) outside-edge binding to the sugar-phosphate backbone of the

18   helix through electrostatic interactions and (iii) groove binding at either the major or minor groove

19   *via* hydrophobic interactions and hydrogen bonding.[48] The sufficient evidences were necessary to

20   predict the main DNA-binding modes. Thus, the DNA-binding behavior and the possible DNA-

21   binding modes of **1-4** toward CT-DNA were intensively investigated by many methods.

22   **3.2.1. Electronic absorption titration.** The changes observed in electronic absorption spectra

23   of the complexes upon addition of DNA concentration are capable to predict their possible DNA-

24   binding modes. Ethidium bromide (EB) which is known as a DNA intercalating agent is used as a

1   reference. Hypochromic effect associated with redshift arises from an intercalative mode involving

2   the strong $\pi \to \pi^*$ stacking interaction between the planar aromatic ligand of the complexes and DNA

3   base pairs.[49,50] Conversely, hyperchromic effect may attribute to two possible causes; (i) the

4   complexes can bind with DNA *via* external contact (electrostatic binding)[51] or (ii) they partially

5   uncoil the DNA helical structure and make more bases embedding in DNA exposed.[52]

6   These interactions involve with non-intercalative modes causing the alteration of the DNA duplex

7   structure.[53] Absorption spectra of **1-4** exhibit the absorption bands in the range of 200−350 nm which

8   are assigned to $\pi \to \pi^*$ intraligand transitions (Fig. 4).[54] Upon titration with CT-DNA at the

9   [Complex]/[DNA] ratios of 0.67−5.00, a decrease in absorbance (hypochromism) with redshift is

10 observed in the spectra of all complexes. This behavior is most likely similar to that observed for a

11 classical intercalator EB (Fig. 4a) but contrast to the starting compounds[12] and other related

12 complexes of amidino-*O*-alkylurea derivatives which have been reported as non-intercalating agents

13 (Table 3).[10,55-57]

14   **"Fig. 4. Should be inserted here"**

15   The binding strength of the complexes with CT-DNA can be evaluated by the values of intrinsic

16 binding constant (K_b) which are obtained by monitoring the change in absorbance at 302 nm for **1**,

17 204 nm for **2**, 300 nm for **3** and 203 nm for **4**. The calculated K_b values are found in the order of

18 EB > **2** > **4** > **1** > **3**. In comparison with their starting compounds which bind to DNA through non-

19 intercalative interactions, all four complexes have higher binding potential. Moreover, they also show

20 better binding strength than other related compounds (Table 3). Such a result indicates that the

21 incorporation of the L^1 or L^2 ligands with the *N,N*-heterocyclic ligands is capable to enhance the

22 DNA interacting efficiency.

23   **"Table 3 Should be inserted here"**

To compare the DNA-binding strength of all four complexes in the present work, their K_b values are considered. In general, the degree of intercalative property of a complex depends on the existing aromatic heterocyclic ring which can insert and stack between the base pairs of DNA. The extension of planarity in the intercalating ligand may strengthen the interaction of the complex with DNA.[58] The obtained results suggest that the complexes in our system can bind to DNA through an intercalative mode with different binding potential. The higher K_b values of the complexes containing phen (**2** and **4**) than the complexes containing bipy (**1** and **3**) may be due to a greater planar area and extended π system of phen than bipy. Hence, phen provides more planarity for **2** and **4** and then gives stronger intercalative interaction with DNA than **1** and **3**.

Complex **3** gives the lowest K_b value meaning to its weakest DNA-binding strength. This may be caused by its structural feature proposed as octahedron according to the spectroscopic results (electronic absorption and EPR). Such a geometry makes the molecule of **3** has less planarity, thus resulting in weaker interactions with DNA than the remaining three compounds (**1**, **2** and **4**) proposed as a square planar. To confirm their DNA-binding behaviors, it is necessary to carry out further experiments.

3.2.2. Viscometric measurements. To further investigate on DNA-binding modes of the complexes, viscometric assay concerning the measurement on the flow time of CT-DNA solutions with increasing amount of the complexes was carried out. Basically, partial and/or non-classical intercalation of the complexes may bend (or kink) the DNA helix, resulting in the reduction of the effective length, and concomitantly its viscosity.[59] Fig. 5 illustrates the plot of the relative viscosity of DNA in the presence and absence of the complexes. Ethidium bromide (EB), an intercalator used as a reference, can enhance the relative viscosity of DNA in the [EB]/[DNA] ratios of 0.0–0.6, due to increasing in the separation of DNA base pairs and lengthening in the DNA helix upon intercalation. When the [EB]/[DNA] ≥ 0.8, the relative viscosity is nearly constant because the binding sites on DNA may reach the saturation. In the presence of the complexes **1-4**, two different behaviors

1 depending on the [Complex]/[DNA] ratios are observed. Firstly, the reduction in the relative

2 viscosity of DNA which shows the opposite trend to EB is observed in the range of

3 [Complex]/[DNA] = 0.0–1.2 for **1**; 0.0–0.6 for **2**; 0.0–1.4 for **3** and 0.0–0.8 for **4** (Fig. 5). Such a

4 behavior points to a non-intercalative binding mode. Lastly, an enhancement of the relative viscosity

5 of DNA is observed when the [Complex]/[DNA] ratios increase from 1.2–2.0 for **1**; 0.6–2.0 for **2**;

6 1.4–2.0 for **3** and 0.8–2.0 for **4**. The higher [Complex]/[DNA] ratios give the similar results as EB at

7 low concentration, suggesting that the complexes have changed their DNA-interacting behaviors to

8 be an intercalative binding mode.

9 **"Fig. 5. Should be inserted here"**

10 It is noticed that the effects of **1-4** on the DNA viscosity are different for both decreasing and

11 increasing ranges. In the decreasing range, complexes **1** and **3** predominantly show the broader range

12 of the [Complex]/[DNA] ratios with more reducing degree of the DNA viscosity than **2** and **4**. In the

13 increasing range, complexes **2** and **4** clearly exhibit progressive enhancement of the viscosity close to

14 EB in the wider range of the [Complex]/[DNA] ratios than **1** and **3**. Under this experimental

15 condition, the results guide that an intercalative interaction is possible to be a major DNA-binding

16 mode for the complexes containing phen (**2** and **4**). In contrast, non-intercalative interactions *i.e.*

17 electrostatic interaction, partial intercalation and/ or groove binding may be a main binding mode for

18 the complexes containing bipy (**1** and **3**). These behaviors denote that the DNA-binding interactions

19 of the complexes depend on the [Complex]/[DNA] ratios.

20 **3.2.3. Circular dichroism spectra.** The effect of metal complexes on the DNA secondary

21 structure can provide good evidence about their potential interactions with the biomolecules. To

22 observe these changes, circular dichroism (CD) signals which are quite sensitive to the DNA-binding

23 mode[60] were determined at the [Complex]/[DNA] ratios of 0.5 and 1.0. Generally, the CT-DNA

24 typed B-form shows CD signal with two characteristic bands including a positive band at 275 nm

1   attributable to base stacking and a negative band at 245 nm arising from the right-handed helicity of

2   DNA.[61] Observed modifications of either a change in the band position or intensity, or even both in

3   the CD spectra of DNA in the presence of the complexes correlate to their interactions. The simple

4   electrostatic interaction or groove binding between the complexes and DNA causes less or no

5   perturbation on the base stacking and helicity bands, whereas the classical intercalation can stabilize

6   the double helical conformation of B-DNA and enhance the intensities of both CD bands, as

7   observed for the classical intercalator ethidium bromide (EB) (Fig. S6a).

8   **"Fig. 8. should be inserted here"**

9   In this study, the characteristic CD bands of all complexes alone are almost unobservable. After

10   incubation of the complexes in the presence of DNA, the changes in CD spectra of DNA are

11   observed. It indicates some modifications in the secondary structure of DNA by **1-4** (Fig. S6b-e). The

12   variations of wavelength ($\Delta\lambda_{max/min}$) and ellipticity ($\Delta\theta_{max/min}$) for both positive and negative bands

13   are listed in Table 4. Addition of **1** gradually decreases in the ellipticity signals of both CD bands

14   along with the redshift (Fig. S6b). The similar modification can also be found for complex **3** (Fig.

15   S6d). On the other hand, complexes **2** and **4** produce a significant increase in the intensity of the

16   positive band with small redshift and a slight decrease in that of the negative band (Fig. S6c and e).

17   **"Table 4 Should be inserted here"**

18   These observable effects of **1-4** on the DNA structure suggest that their interactions with DNA

19   may be different. Under the condition in this study, the small perturbation of **1** and **3** clearly

20   opposites to the effect of EB (Fig. S6a); therefore, their interactions with DNA are proposed as non-

21   intercalative modes. The effect of **1** and **3** on DNA is also analogous to the starting complexes

22     $[Cu(L^1)Cl_2]_2$ and $[Cu(L^2)Cl_2]_2$.[12] While the effect of **2** and **4** are dissimilar to **1** and **3** but similar to

23   some metal complexes containing 1,10-phenanthroline.[57,58] A great increase in the intensity of the

24   positive band possibly involves the intercalative interaction stabilized by π-π stacking interaction of

1   the complexes on base pairs of the double helix.[58] Whereas, a moderate decrease in the intensity of

2   the negative band is indicative of unwinding the helical DNA structure by the complexes, leading to

3   loss some of helicity and encourages the transformation to more A-like DNA conformation.[57]

4   **3.2.4. DNA-melting study.** Additional evidence for the possible DNA-binding behavior of **1-4**

5   can be obtained from thermal denaturation study. When the temperature of DNA solution increases,

6   the double-stranded DNA slowly dissociates to single strands mirrored by the hyperchromic effect at

7   259 nm. Interaction of a small molecule with DNA can be observed from the alteration of the melting

8   temperature (T_m) depending on its binding affinity. It is known that an intercalating molecule gives

9   rise to stabilization of the DNA helix indicated by a high increase of T_m value while a non-

10   intercalating molecule providing lower DNA-affinity may produce a small change of T_m value ($\Delta T_m <$

11   3 °C).[10,12,62]

12   All four complexes reveal the tendency of increasing the T_m of DNA (81.1 °C) with increasing in

13   the [Complex]/[DNA] ratios (Fig. S7 and Table 5), indicating the interaction between DNA and the

14   complexes. Noticeably, a degree of enhancement of ΔT_m directly depends on the [Complex]/[DNA]

15   ratios of each compound. The small change of ΔT_m induced by **1** occurs at the [Complex]/[DNA]

16   ratios of 0.5 – 1.5. In addition, the similar behavior to the former compound can also be observed at

17   the [Complex]/[DNA] ratios of 0.5 for **2** and 0.5 – 1.0 for **4**, suggesting that the DNA-binding mode

18   of the **1**, **2** and **4** at those appropriate [Complex]/[DNA] ratios is most likely non-intercalation. When

19   the [Complex]/[DNA] ratio is reached at 2.0, the three compounds again show an enhancement of T_m

20   with $\Delta T_m > 3$ °C indicating a different DNA-binding behavior, probably intercalation. Differently,

21   the T_m values of DNA solutions in the presence of **3** gradually increase upon increasing the

22   [Complex]/[DNA] ratios with $\Delta T_m < 3$ °C, pointing that a major DNA-binding mode may be non-

23   intercalation. Such a result agrees well with the evidence obtained from viscosity measurements and

24   circular dichroism spectroscopy.

2 Noticeably, the ΔT_m values at the [Complex]/[DNA] ratio = 2.0 are found in the trend of **2** > **4** >

3 **1** > **3** which correlates to their DNA-binding affinity.[62] In comparison with their starting compounds

4 $[Cu(L^1)Cl_2]_2$ and $[Cu(L^2)Cl_2]_2$ ($\Delta T_m = 0.3$–$1.3°C$) under the same condition,[12] the higher ΔT_m values

5 of **1-4** are observed. This may imply that all complexes in this system containing the *N,N*-

6 heterocyclic ligands can bind to DNA more strongly than their initial compounds.

7 **3.2.5. Quenching of DNA-ethidium bromide fluorescence by the copper(II) complexes.**

8 Fluorescence spectroscopy is a simple method which shows high sensitivity and selectivity. It is

9 widely used to determine the interaction mode of DNA and the complexes. Ethidium bromine (EB) is

10 one of the most fluorescence indicators that can emit fluorescence when bound with DNA (EB-DNA

11 complex) at 593 nm because of strong intercalative binding into the adjacent of DNA base pairs. The

12 binding of another molecule to DNA can quench the emission intensity of EB either by displacement

13 the EB and/or by accepting the exited state electron from EB through a photo-electron transfer

14 mechanism.[63,64] The solutions of **1-4** in 3% MeOH/Tris-buffer at pH = 7.2 in the absence and

15 presence of DNA show no fluorescence at room temperature. Upon addition of the complexes to the

16 EB-DNA system with the [Complex]/[DNA] ratios of 0.1–1.0, all complexes can moderately

17 decrease the intensity of EB-DNA complex (Fig. S8), suggesting that the DNA-binding of all

18 complexes occurs *via* probably (i) competing with EB at the same binding sites and/or (ii) interacting

19 at different sites as shown below.[65,66]

20 (i) CuL + DNA−EB $\rightleftharpoons$ DNA−CuL + EB

21 and/or

22 (ii) CuL + DNA−EB $\rightleftharpoons$ EB−DNA−CuL

23 Principally, if the [Complex]/[DNA] ratio < 100 is used and the quenching efficiency > 50% is

24 received, the compound will bind to DNA through intercalative mode.[67] In this study using the

1   [Complex]/[DNA] ratios of 0.1–1.0, the EB-DNA emission intensities caused by the complexes

2   decrease less than 50% (Fig. 6), indicating that they may not interact with the double strand at the

3   same sites of EB and not replace EB. Hence, the complexes in this system possibly interfere the

4   EB-DNA interaction and/or involve the formation of a non-fluorescence [EB−DNA−CuL] species as

5   described in pathway (ii). Moreover, the linearity Stern-Volmer plots (Eq. 2) as shown in insets of

6   Fig. S8 indicates that the quenching reaction is mainly carried out *via* static quenching process[68]

7   which involves in the formation of a non-flourescence species as described in pathway (ii). Non-

8   intercalation may be their major DNA-binding mode at low concentration. The quenching ability of

9   complexes **1-4** evaluated by the Stern-Volmer quenching constant (K_{sv}) are in the order of **2**

10 (1.07×10^4 M^{-1}) > **4** (3.24×10^3 M^{-1}) > **1** (1.76×10^3 M^{-1}) > **3** (1.49×10^3 M^{-1}) corresponding to their K_b

11 values (see Table 3).

12   **"Fig. 6. Should be inserted here"**

13   **3.2.6.   Determination of the DNA-binding stoichiometry of the copper(II) complexes.**

14 Determination of DNA-binding stoichiometry of the copper(II) complexes is another method to

15 further clarify the binding mode. The stoichiometric ratio is expressed by the Cu (mmol)/DNA (mol

16 base). These values can be analysed by considering the stoichiometric ratios of copper(II) aqua ion

17 [Cu(H$_2$O)$_6$]$^{2+}$ (ratio > 150) and copper(II)-dipeptide complexes (ratio < 42).[22] A large difference in

18 stoichiometry of the two compounds can be assumed that their DNA-interactions are dissimilar. The

19 positively charged copper(II) aqua ion interacts with DNA probably in a less selective interaction

20 such as electrostatic attractions with the negatively charged phosphate groups. On the other hand, the

21 significantly smaller stoichiometry of the copper(II)-dipeptide complexes possibly suggest more

22 selective DNA-binding mode such as intercalation. In this work, the obtained stoichiometry of **1-4** at

23 the [Complex]/[DNA] ratio of 1.0 exhibits 64, 77, 59 and 68 Cu (mmol)/DNA (mol base),

respectively, which are slightly higher than that of copper-dipeptide complexes. Such a result implies that the four compounds may bind to DNA *via* non-intercalative mode under this condition.

3.2.7. Possible DNA-binding modes. Results from various efficient techniques as described above are useful for the prediction of the possible DNA-binding interaction of the complexes **1**-**4**. All evidences suggest that the four copper(II) complexes are capable to interact with the DNA double helix *via* both non-intercalative and intercalative modes depending on the [Complex]/[DNA] ratio.

At the [Complex]/[DNA] ratio < 1.0, the main DNA-binding behavior is expected to be non-intercalation mode. Upon increasing in the amount of the complexes, their binding mode are changed to intercalative interactions, at the [Complex]/[DNA] ratios > 1.0 for **2** and **4**, > 1.5 for **1** and > 2.0 for **3**. Such a behavior may arise from the stability of the interactions between DNA and each complex. Changes in the binding modes of **2** and **4** from non-intercalation to intercalation occur at the lower ratios than **1** and **3**. This supports the fact that the complexes containing 1,10-phenanthroline tend to bind to DNA *via* intercalation. In the case of **3**, its structural feature is least planar, thus difficult to interact with DNA through intercalation.
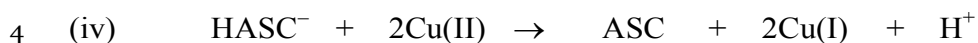
3.3. DNA cleavage studies of copper(II) complexes with pBR322 DNA

3.3.1. Gel electrophoresis. The DNA cleavage activities of the copper(II) complexes were investigated by determining the conversion of the plasmid DNA which is mainly in the supercoiled form (Form I) to the nicked circular (Form II) and linear forms (Form III) by electrophoresis technique. When electrophoresed, the three forms of DNA are separated by their different mobility rate on gel. The relatively fast migration will be observed for Form I. Form II is the bulkiest, thus it will move slowest while Form III will migrate between Forms I and II. The DNA cleavage activities of the complexes **1**-**4** toward plasmid pBR322 DNA are shown in Fig. 7.

"Fig. 7. Should be inserted here"

1   Upon increasing the complex concentration from 200 to 800 µM, increases in DNA Form II are

2   observed in the electrophoretic bands. The complexes containing bipy (**1** and **3**) induce a slight

3   increase in the band intensities of Form II while the complexes containing phen (**2** and **4**) are capable

4   to considerably enhance (Fig. S9). However, all complexes can partially cleave the DNA Form I to

5   Form II. The extent of the DNA cleavage potential at the final concentration of the complexes

6   calculated by Eq. 3 follows the order of **2** (57.70%) > **4** (50.70%) > **1** (31.60%) > **3** (9.37%).

7   Furthermore, the oxidative cleavage properties of the complexes were investigated by addition of

8   H_2ASC to mimic the reducing environment found inside the cells. The role of H_2ASC is to reduce

9   Cu(II) to Cu(I) which then induce the formation of the reactive oxygen species (ROS) that finally

10   cleave DNA. According to the different DNA-binding potential of the four complexes, an appropriate

11   concentration of each complex is 10-400 µM for **1** and **3** and 0.1-4.0 µM for **2** and **4** in the presence

12   of H_2ASC (100 µM) as demonstrated in Fig. 8. H_2ASC alone does not cause DNA cleavage (lane 2,

13   Fig. 8). In the presence of **1** and **3**, Form II is gradually increased from the concentration of 10 to 200

14   µM (lanes 3-9, Fig. 8a and 8c, respectively). At 400 µM (lane 10), complex **1** can totally cleave DNA

15   Forms I to Form II but complex **3** produces 52.77% of Form II (Fig. S10a and c). In the case of **2** and

16   **4**, both complexes significantly cleave Forms I to Form II up to 1.0 µM, then Form II is progressively

17   occurred from 2.0 µM (Fig. 8b and 8d). However, their DNA-cleavage potential is different as seen

18   by the percentage of Form III of 31.1 and 6.55 in the presence of **2** and **4**, respectively (Fig. S10b and

19   d).

20   **"Fig. 8. should be inserted here"**

21   Such a behavior leads us to assume that the DNA cleavage behaviors of all complexes in the

22   presence of H_2ASC are possibly involved in the oxidative process by generating the reactive oxygen

23   species (ROS) such as hydrogen peroxide (H_2O_2), hydroxyl radical ($OH^•$), singlet oxygen ($^1O_2$) or

24   superoxide (O_2^-) which can cleave DNA.[69] The major role of these copper(II) complexes is based on

1 the enzymatic properties of copper which is important to the proposed mechanism of the *in situ*

2 formation of H_2O_2 as shown below.[70,71]

3 (iii) $H_2ASC + H_2O \rightleftharpoons HASC^- + H_3O^+$

4 (iv) $HASC^- + 2Cu(II) \rightarrow ASC + 2Cu(I) + H^+$

5 (v) $2Cu(I) + O_2 + 2H^+ \rightarrow 2Cu(II) + H_2O_2$

6 (vi) $HASC^- + O_2 + H^+ \rightarrow ASC + H_2O_2$

7   Finally, hydrogen peroxide reacts with another equivalent of the Cu(I) through the Fenton

8 reaction (vii) producing a highly reactive species, hydroxyl radical responsible for DNA oxidative

9 damage.[70] This situation can be found for other copper(II) complexes of which their DNA cleavage

10 properties are increased by adding the reducing agent such as ascorbic acid.[12,72-74]

11 (vii) $Cu(I) + H_2O_2 \rightarrow Cu(II) + OH^- + OH^\bullet$
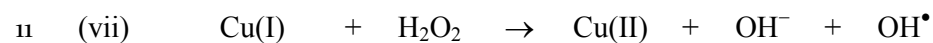
12   In summary, all four complexes in this work can produce the DNA strand scission in the

13 presence of H_2ASC *via* the oxidative pathway with the order efficiency of **2 > 4 > 1 > 3**

14 corresponding to their DNA-binding affinities.

15   **3.3.2. Effect of the complexes on DNA morphology.** Additional investigation on interactions

16 of the copper(II) complexes with DNA can be clearly visualized by atomic-force microscopy (AFM).

17 The morphology changes of the plasmid pBR322 DNA induced by the complexes would be observed

18 in the AFM images. The appropriate condition of each complex utilized to gain the AFM images is

19 different, depending on their DNA cleavage reactivity. According to the electrophoretic experiments,

20 the plasmid DNA treated by the complexes in the presence of H_2ASC (100 µM) in HEPES-buffer

21 was carried out in two conditions to perform the AFM images (Fig. 9a-f): (i) 400 µM for **1** and **3** and

22 (ii) 4 µM for **2** and **4**. After incubation, the supercoiled DNA alone (Form I) is not affected by

23 H_2ASC (Fig. 9b). When treated by complex **1**, the supercoiled DNA is perfectly converted to the

24 open circular DNA (Fig. 9c) while complex **3** shows partial DNA cleavage (Fig. 9e). The linear DNA

1   can be found on the AFM images when treated by the complexes **2** and **4**. Noticeably, complex **2** can

2   effectively cut the DNA strands into smaller linear form (Fig. 9d) than complex **4** (Fig. 9f). Results

3   from AFM images are consistent with those obtained from the electrophoresis method (see lane 10 in

4   Fig. 8).

5   **"Fig. 9. Should be inserted here"**

6   **3.4. Anticancer activity of the copper(II) complexes**

7   The four complexes **1−4** were further examined their *in vitro* cytotoxicity against three human cancer

8   cell lines including small cell lung carcinoma (NCI-H187), the oral cavity carcinoma (KB) and the

9   breast adenocarcinoma (MCF-7) by resazurin microplate assay. Their anticancer activities are

10   summarized in Table 6.

11   **"Table 6 should be inserted here"**

12   The obtained results are revealed that the complexes in the present work have potential to inhibit

13   the growth of the tested cancer cells but different cytotoxic activity. However, complex **3** is active

14   toward only NCI-H187 cells. According to their IC_{50} values, the degree of the anticancer activity has

15   been found to be in the order of **2** > **4** > **1** > **3**. It is noticed that compounds **2** and **4** which contain the

16   phenanthroline ligand show higher activity than compounds **1** and **3** which contain the bipyridine

17   ligand. These observations are in agreement with their potential DNA-binding and cleaving

18   properties. To compare with the starting complexes $[Cu(L^1)Cl_2]_2$ and $[Cu(L^2)Cl_2]_2$, the complexes

19   containing the additional *N,N*-heterocyclic ligands exhibit a significantly greater activity (Table 6).

20   Further comparisons are made with free *N,N*-heterocyclic molecules (bipy and phen) and cisplatin at

21   the same condition as done for **1-4**. Compound **1** is considerably more active against the KB and

22   MCF-7 cell lines but lower activity against the NCI-H187 cell line than the free bipy. While,

23   compound **3** has a lower cytotoxicity than the free bipy which may arise from its structural feature. In

24   the case of phen, both **2** and **4** show such a dramatically better anticancer activity than the free phen.

Such a behavior suggests that phen together with L^1 or L^2 in the compounds help to improve the cytotoxic potential. Moreover, the cytotoxic properties of all complexes, except for **3**, are considerably greater than cisplatin. Complex **3** displays much lower cytotoxicity than the remaining three compounds. This may be due to the fact that it adopts a different geometry (octahedron) from the others (square planar). Such a result points that the factors to control the anticancer activity are not only the types of ligands but also the coordination geometry.

3.5. Antibacterial activity studies

The previous reports revealed the interesting antibacterial activities of some copper(II) complexes of amidino-*O*-alkylurea derivatives against Bacillus,[75] *E.coli*,[12,76,77] *K. Pneumonia* and *P. mirabilis*,[76] *Salmonella* and *Campylobacter*.[10,12,77] Herein, our compounds containing amidino-*O*-methylurea derivatives and the *N,N*-heterocycles were further tested the *in vitro* antibacterial properties against *E. coli*, *Salmonella* and *Campylobacter* by disc diffusion method. Their antibacterial activities were evaluated by the value of minimum inhibitory concentrations (MICs) (Table 7).

"Table 7 should be inserted here"

Compound **2** is found to have the highest antibacterial activity toward the tested bacteria. Compound **4** also can inhibit the growth of all three bacteria, but lower activity than **2**. Compound **1** is only active against *Campylobacter*. On the other hand, compound **3** gives the lowest potential with no antibacterial activity toward all tested bacteria. Although their starting compounds are able to inhibit the growth of the three bacteria, but they display considerably higher MIC values than **1** (for *Campylobacter*), **2** and **4**. Such evidence strongly confirms that the existence of the *N,N*-heterocyclic ligand particularly phen together with L^1 or L^2 can improve their antibacterial activities. Nevertheless, compound **3** is inactive toward all tested pathogenic bacteria. This may arise from its proposed structural geometry as a distorted octahedron which may be inappropriate to interact with

1   the cells. Such a behavior is perfectly consistent with their DNA interaction potential as well as

2   cytotoxicity.

3   Enrofloxacin, a well-known antibacterial drug, was also tested as a reference to compare with the

4   complexes in this system. As expected, it exhibits much higher activity against the three tested

5   bacteria. Although our compounds have less antibacterial potential than enrofloxacin, they still reveal

6   a better inhibitory effect than their starting compounds. Therefore, it is promising to develop the

7   copper(II) compounds based on amidino-*O*-methylurea and its derivatives as an antibacterial agent

8   for a series of human-food poisoning bacteria in the future.

9   **4. Conclusions**

10 In this work, we have designed and synthesized four new copper complexes of amidino-*O*-

11 methylurea (L^1) and *N*-(benzyl)-amidino-*O*-methylurea (L^2) containing the *N,N*-heterocyclic ligands

12 (bipy and phen), $[Cu(L^1)(bipy)]Cl_2$ (**1**), $[Cu(L^1)(phen)]Cl_2$ (**2**), $[Cu(L^2)(bipy)Cl_2]$ (**3**) and

13 $[Cu(L^2)(phen)]Cl_2$ (**4**). Compounds **1**, **2** and **4** are proposed to adopt a square planar CuN_4 geometry

14 while **3** is possibly a distorted octahedron. All complexes show DNA-binding properties with two

15 possible modes depending on the complex concentration; non-intercalation at low concentration and

16 intercalation at high concentration. In addition, they exhibit DNA cleaving efficiency toward the

17 supercoiled DNA possibly *via* oxidative cleavage mechanism. Their anticancer activities toward the

18 small cell lung carcinoma (NCI-H187), the oral cavity carcinoma (KB) and the breast

19 adenocarcinoma (MCF-7) is better than the starting complexes $[Cu(L^1)Cl_2]_2$ and $[Cu(L^2)Cl_2]_2$,

20 particularly NCI-H187. Furthermore, the antibacterial activity against three gram negative bacteria

21 (*E. coli, Salmonella and Campylobacter*) of **2** and **4** is considerably greater than **1** and **3**. According

22 to their DNA-binding and cleaving properties as well as their anticancer and antibacterial potential,

23 the activity follows in the order of **2** > **4** > **1** > **3**. Such a result suggests that the complexes of ligand

24 L^1 or L^2 and the planar phen display significantly higher cytotoxicity than those containing bipy. This

1   may come from the fact that phen is more hydrophobic; hence assisting **2** and **4** to diffuse through the

2   cancer and bacterial cell membrane easier.

3   In summary, the DNA-interacting property and cytotoxicity of the complexes depend on the

4   ligand type (L^1 or L^2), structural features and hydrophobicity. Interestingly, this complex system is

5   still a challenge to further study on the development as a new generation agent for human cancer

6   therapy and/or human food-poisoning treatment.

7   **Acknowledgements**

15   **References**

16   1   B. Rosenberg, L. van Camp, J. E. Trosko and V. H. Mansour, *Nature*, 1969, **222**, 385−386.

17   2   P. J. Loehrer and L. H. Einhorn, *Ann. Intern. Med.*, 1984, **100**, 704−713.

18   3   A. Eastman, Cisplatin, in: B. Lippert (Ed.), *Chemistry and Biochemistry of a Leading*

19   *Anticancer Drug*, VHCA & Wiley-VCH, Zurich & Germany, 1999, pp. 111−134.

20   4   J. R. R. Frausto da Silva and R. J. P. Williams, *The Biological Chemistry of the Element:*

21   *Inorganic Chemistry of Life*, Clarendon Press, New York, 1991, pp. 40−41, 389−399.

22   5   T. Ma, J. Xu, Y. Wang, H. Yu, Y. Yang, Y. Liu, W. Ding, W. Zhu, R. Chen, Z. Ge, Y. Tan,

23   L. Jia and T. Zhu, *J. Inorg. Biochem.*, 2015, **144**, 38−46.

6   P. P. Silva, W. Guerra, G. C. Santos, N. G. Fernandes, J. N. Silveira, A. M. C. Ferreira, T. Bortolotto, H. Terenzi, A. J. Bortoluzzi, A. Neves and E. C. Pereira-Mai, *J. Inorg. Biochem.*, 2014, **132**, 67−76.

7   N. Raman, R. Mahalakshmi and L. Mitu, *Spectrochim. Acta, Part A*, 2014, **131**, 355−364.

8   P. Hubberstey, U. Suksangpanya and C. Wilson, *CrystEngComm*, 2000, **26**, 141−145.

9   U. Suksangpanya, A. J. Blake, P. Hubberstey, D. J. Parker, S. J. Teat and C. L. Wilson, *CrystEngComm*, 2003, **5**, 10−22.

10   U. Chaveerach, A. Meenongwa, Y. Trongpanich, C. Soikum and P. Chaveerach, *Polyhedron*, 2010, **29**, 731−738.

11   M. J. Begley, P. Hubberstey and C. H. M. Moore, *J. Chem. Research (S)*, 1986, 172−173.

12   A. Meenongwa, R. F. Brissos, C. Soukum, P. Chaveerach, P. Gamez, Y. Trongpanich and U. Chaveerach, *New J. Chem.*, 2015, **39**, 664−675.

13   S. Iglesias, N. Alvarez, M. H. Torre, E. Kremer, J. Ellena, R. R. Ribeiro, R. P. Barroso, A. J. Costa-Filho, M. G. Kramer and G. Facchin, *J. Inorg. Biochem.*, 2014, **139**, 117−123.

14   A. Galani, E. K. Efthimiadou, G. Mitrikas, Y. Sanakis, V. Psycharis, C. Raptopoulou, G. Kordas and A. Karaliota, *Inorg. Chim. Acta*, 2014, **423**, 207−218.

15   J. D. C. Almeida, D. A. Paixão, I. M. Marzano, J. Ellena, M. Pivatto, N. P. Lopes, A. M. D. C. Ferreira, E. C. Pereira-Maia, S. Guilardi and W. Guerra, *Polyhedron*, 2015, **89**, 1−8.

16   A. Meenongwa, U. Chaveerach and K. Siriwong, *Inorg. Chim. Acta*, 2011, **366**, 357−365.

17   J. Marmur, *J. Mol. Biol.*, 1961, **3**, 208−218.

18   M. F. Reichmann, S. A. Rice, C. A. Thomas and P. Doty, *J. Am. Chem. Soc.*, 1954, **76**, 3047−3053.

19   A. Wolfe, G. H. Shimer and T. Meehan, *Biochemistry,* 1987, **26**, 6392−6396.

20   G. Cohen and H. Eisenberg, *Biopolymers*, 1969, **8**, 45−49.

21   J. R. Lakowicz and G. Weber, *Biochemistry*, 1973, **12**, 4161−4170.

22   G. Facchin, E. Kremer, D. A. Barrio, S. B. Etcheverry, A. J. Costa-Filho and M.H. Torre, *Polyhedron*, 2009, **28**, 2329−2334.

23   M. F. Shubsda, J. Goodisman and J. C. Dabrowiak, *J. Biochem. Biophys. Methods*, 1997, **34**, 73−79.

24   M. N. Patel, P. A. Dosi and B. S. Batt, *Polyhedron*, 2010, **29**, 3238−3245.

25   J. O. Brien, I. Wilson, T. Orton and F. Pognan, *Eur. J. Biochem.*, 2000, **267**, 5421−5426.

26   M. J. O′Neill, D. H. Bray, P. Boardmann, J. D. Phillipson and D. C. Warhurst, *Planta Med.*, 1985, **51**, 394−398.

27   C. H. Collins and P. M. Lyne, *Microbiological Methods*, University Park Press, Baltimore, 1970, pp. 422.

28   E. J. L. Lana, F. Carazza and J. A. Takahashi, *Agric. Food Chem.*, 2006, **54**, 2053−2056.

29   R. S. Kumar, K. Sasikala and S. Arunachalam, *J. Inorg. Biochem.*, 2008, **102**, 234−241.

30   G. Marcon, S. Carotti, M. Coronnello, L. Messori, E. Mini, P. Orioli, T. Mazzei, M. A. Cinellu and G. Minghetti, *J. Med. Chem.*, 2002, **45**, 1672−1677.

31   R. A. Macleod, *J. Biol. Chem.*, 1952, **197**, 751−761.

32   C. Krishmanurti, L. A. Saryan and D. H. Petering, *Cancer Res.*, 1980, **40**, 4092−4099.

33   P. R. Reddy, A. Shilpa, N. Raju and P. Raghavaiah, *J. Inorg. Biochem.*, 2011, **105**, 1603-1612.

34   M. Satterfield and J. S. Brodbelt, *Inorg. Chem*. 2001, **40**, 5393−5400.

35   J. Shen and J. Brodbelt, *J. Mass. Spectrom.*, 1999, **34**, 137−146.

36   B. Louis, C. Detoni, N. M. F. Carvalho, C. D. Duarte and O. A. C. Antunes, *Appl. Catal., A*, 2009, **360**, 218−225.

37 R. Starosta, U. K. Komarnicka, M. Sobczyk and M. Barys, *J. Lumin.*, 2012, **132**, 1842−1847.

38 W. K. Musker and M. S. Hussain, *Inorg. Chem.*, 1969, **8**, 528−536.

39 B. J. Hathaway, *J. Chem. Soc., Dalton Trans.*, 1972, 1196−1199.

40 P. Comba, N. F. Curtis, G. A. Lawrance, A. M. Sargeson, B. W. Skelton and A. H. White, *Inorg. Chem.*, 1986, **25**, 4260−4267.

41 I. M. Proctor, B. J. Hathaway and P. Nichols, *J. Chem. Soc. A.*, 1968, 1678−1684.

42 D. N. Zimmerman and J. L. Hall, *Inorg. Chem.*, 1973, **12**, 2616−2620.

43 B. J. Hathaway and D. E. Billing, *Coord. Chem. Rev.*, 1970, **5**, 143−207.

44 B. A. Goodman and J. B. Raynor, Electron spin resonance of transition metal complexes, in: H.J. Eméleus, A.G. Sharpe (Eds.), *Adv. Inorg. Chem. Radiochem.*, Academic Press, New York, 1970, **13**, pp. 135−362.

45 G. Tabbi, A. Giuffrida and R. P. Bonomo, *J. Inorg. Biochem.*, 2013, **128**, 137−145.

46 J. R. Wasson and C. Trapp, *J. Phys. Chem.*, 1969, **73**, 3763−3772.

47 A. C. Mot, S. A. Syrbu, S. V. Makarov, G. Damian and R. Silaghi-Dumitrescu, *Inorg. Chem. Commun.*, 2012, **18**, 1−3.

48 G. M. Blackburn, M. J. Gait and D. Loakes, Reversible Small Molecule-Nucleic Acid Interactions, in: D.M. Williams (Ed.), *Nucleic acid in chemistry and biology*, RSC Publishing, Cambridge, 3rd ed., 2006, pp. 342−382.

49 L. S. Lerman, *J. Mol. Biol.*, 1961, **3**, 18−30.

50 E. C. Long and J. K. Barton, *Acc. Chem. Res.*, 1990, **23**, 271−273.

51 R. F. Pasternack, E. J. Gibbs and J. Villafranca, *Biochemistry*, 1983, **22**, 2406−2414.

52 G. Pratviel, J. Bernadou and B. Meunier, *Adv. Inorg.Chem.*, 1998, **45**, 251−312.

53 Q. Li, P. Yang, H. Wang and M. Guo, *J. Inorg. Biochem.*, 1996, **64**, 181−195.

54   J. B. Lambert, H. F. Shurvell, L. Verbit, R. G. Cooks and G. H. Stout, *Organic structural analysis*, Macmillan Publishing, New York, 1976.

55   S. P. Devi, R. K. B. Devi, M. Damayanti, N. R. Singh and R. K. H. Singh, *Polyhedron*, 2012, **47**, 1−8.

56   Z. S. Yang, Y. L. Wang and G. C. Zhao, *Anal. Sci.*, 2004, **20**, 1127−1130.

57   T. Gupta, S. Dhar, M. Nethaj and A. R. Chakravaty, *Dalton Trans.*, 2004, 1896−1900.

58   J. Z. Wu, B. H. Ye, L. Wang, L. N. Ji, J. Y. Zhou, R. H. Li, Z. Y. Zhou, *J. Chem. Soc. Dalton.*, 1997, 1395−1401.

59   S. Satyanarayana, J. C. Dabrowiak and J. B. Chaires, *Biochemistry*, 1992, **31**, 9319–9324.

60   D. S. Raja, N. S. P. Bhuvanesh and K. Natarajan, *Inorg. Chim. Acta*, 2012, **385**, 81−93.

61   V. I. Ivanov, L. E. Minchenkova, A. K. Schyolkina and A. I. Poletayev, *Biopolymers*, 1973, **12**, 89−110.

62   G. A. Neyhart, N. Grover, S. R. Smith, W. Kalsbeck, T. A. Fairley, M. Cory and H. H. Thorp, *J. Am. Chem. Soc.*, 1993, **115**, 4423−4428.

63   B. C. Baguley and M. LeBret, *Biochemistry*, 1984, **23**, 937–943.

64   R. F. Pasternack, M. Cacca, B. Keogh, T. A. Stephenson, A. P. Williams and F. J. Gibbs, *J. Am. Chem. Soc.*, 1991, **113**, 6835–6840.

65   E. Nyarko, N. Hanada, A. Habib and M. Tabata, *Inorg. Chim. Acta*, 2004, **357**, 739–745.

66   V. C. Silveira, H. Benezra, J. S. Luz, R. C. Georg, C. C. Oliveira and A. M. C. Ferreira, *J. Inorg. Biochem.*, 2011, **105**, 1692–1703.

67   X. Ling, W. Zhong, Q. Huang and K. Ni, *J. Photochem. Photobiol. B: Biol.*, 2008, **93**, 172–176.

68   J. R. Lakowicz, *Principles of Fluorescence Spectroscopy*, 3rd ed., Plenum Press, New York, 2006, pp. 277–286.

69   B. Halliwell and J. M. C. Gutteridge, *Free Radicals in Biology and Medicine*, Oxford Science Publication, Oxford, 3rd ed, 1999, pp. 42–43.

70   D. S. Sigman and C. H. B. Chen, *Acc. Chem. Res.*, 1986, **19**, 180–186.

71   I. Yamazaki and L. H. Piette, *Biochem. Biophys. Acta*, 1961, **59**, 62–69.

72   M. Ganeshpandian, R. Loganathan, S. Ramakrishnan, A. Riyasdeen, M. A. Akbarsha and M. Palaniandavar, *Polyhedron*, 2013, **52**, 924–938.

73   X. B. Fu, G. T. Weng, D. D. Liu and X. Y. Le, *J. Photochem. Photobiol., A*, 2014, **276**, 83–95.

74   X. B. Fu, J. J. Zhange, D. D. Liu, Q. Gan, H. W. Gao, Z. W. Mao and X. Y. Le, *J. Inorg. Biochem.*, 2015, **143**, 77– 87.

75   O. I. Singh, M. Damayanti, N. R. Singh, R. K. H. Singh, M. Mohapatra and R. M. Kadam, *Polyhedron*, 2005, **24**, 909 – 916.

76   S. P. Devi, R. K. B. Devi, M. Damayanti, N. R. Singh, R. K. H. Singh and R. M. Kadam, *J. Coord. Chem.*, 2011, **64**, 1586–1601.

77   R. Pretumwieng, C. Soikum, P. Chaveerach and U. Chaveerach, *Inorg. Chim. Acta*, 2014, **423**, 421–429.

1   **Figure captions:**
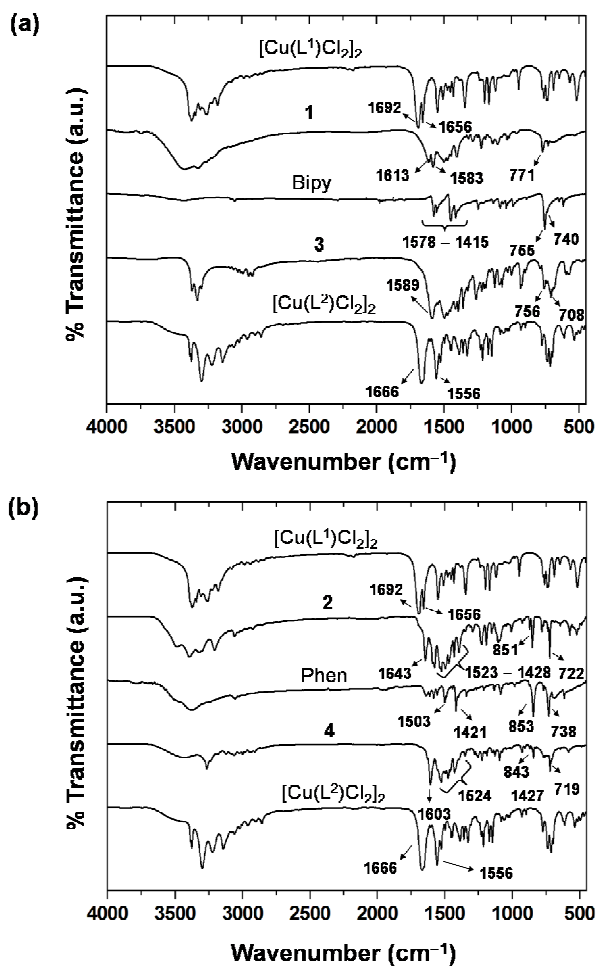
2

3   **Fig. 1** Overlayered FT-IR spectra of (a) **1** and **3**, and (b) **2** and **4** compared with the starting

4   complexes and the secondary chelating *N,N*-heterocyclic ligands (bipy and phen).

5
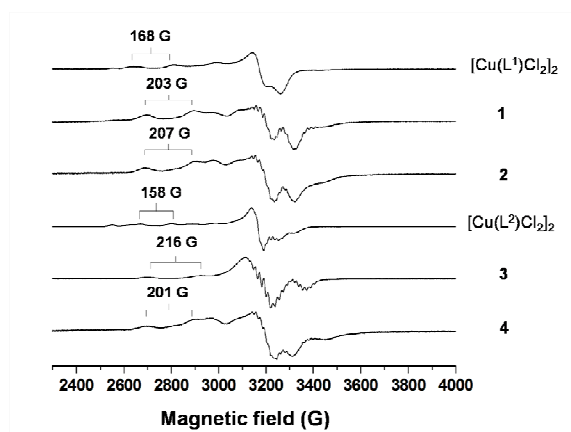
Fig. 2 X-band EPR spectra in a frozen DMSO solution of complexes **1-4** compared with the starting complexes $[Cu(L^1)Cl_2]_2$ and $[Cu(L^2)Cl_2]_2$ at 77 K.
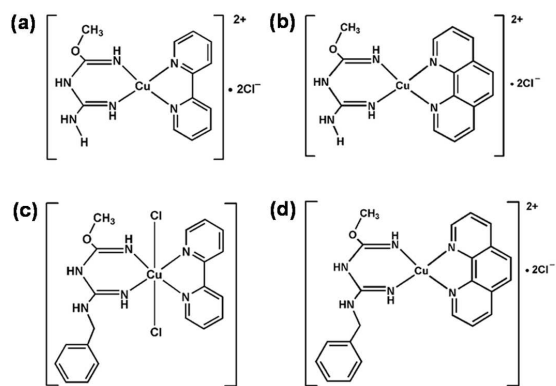
Fig. 3 Possible geometries of (a) **1**, (b) **2**, (c) **3** and (d) **4**.

1

2

3

4
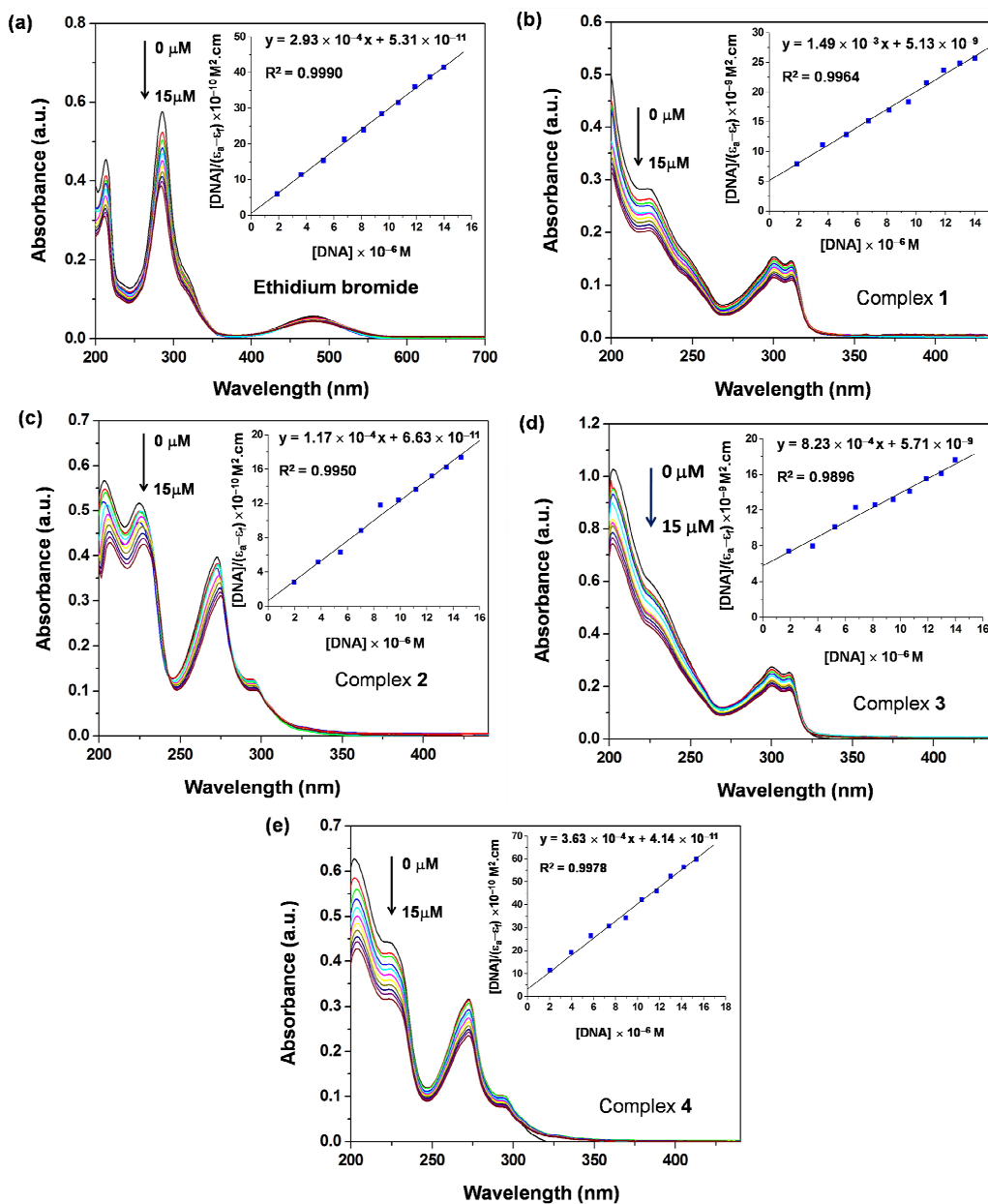
Fig. 4 Absorption spectra of ethidium bromide (a) and the complexes **1-4** (10 μM) (b-e) in the absence (——) and presence of increasing amounts of DNA (2–15 μM) after incubation at 37 °C for 24 h. The arrows show the absorbance changes upon the addition of the DNA concentrations. Insets: Linear plot of $[DNA]/(\varepsilon_a-\varepsilon_f)$ *vs.* [DNA] for the titration of the copper(II) complexes with DNA.

1
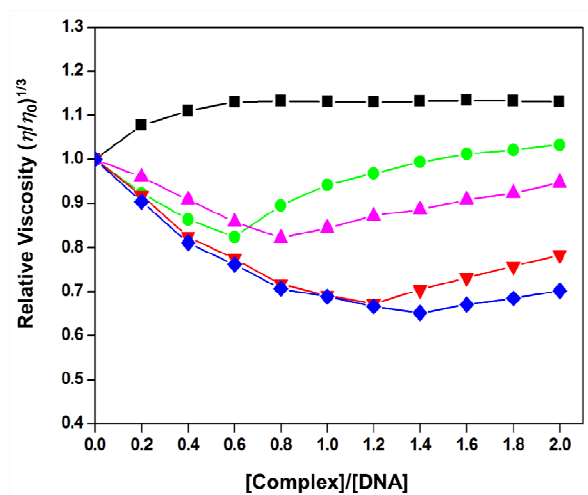
Fig. 5 Influence of increasing amount of ethidium bromide (−■−), complexes 1 (−▼−), 2 (−●−),

3 (−◆−) and 4 (−▲−) on the relative viscosity of CT-DNA (200 μM) at 37 °C.
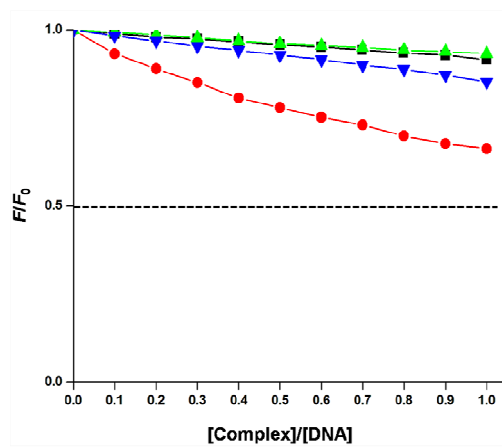
1

2

3   **Fig. 6** Plots of the relative fluorescence quenching of EB-DNA complex treated by **1** (■), **2** (●),

4   **3** (▲) and **4** (▼) at the [Complex]/[DNA] ratios of 0.1–1.0.

5
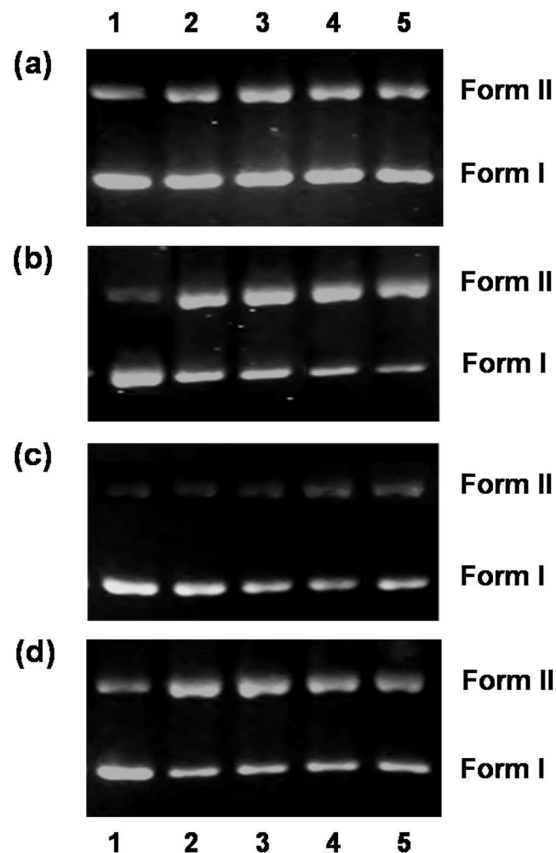
1

2   **Fig. 7** Electrophoretic diagrams of supercoiled pBR322 DNA (0.2 µg, ~30 µM) cleaved by

3   complexes (a) $[Cu(L^1)(bipy)]Cl_2$ (**1**); (b) $[Cu(L^1)(phen)]Cl_2$ (**2**); (c) $[Cu(L^2)(bipy)Cl_2]$ (**3**) and (d)

4    $[Cu(L^2)(phen)]Cl_2$ (**4**) in HEPES-buffer. Incubation at 37 °C for 1 h. Lane 1, plasmid DNA alone;

5   lanes 2–5, DNA + [Complex] (200, 400, 600 and 800 µM, respectively).

6

7
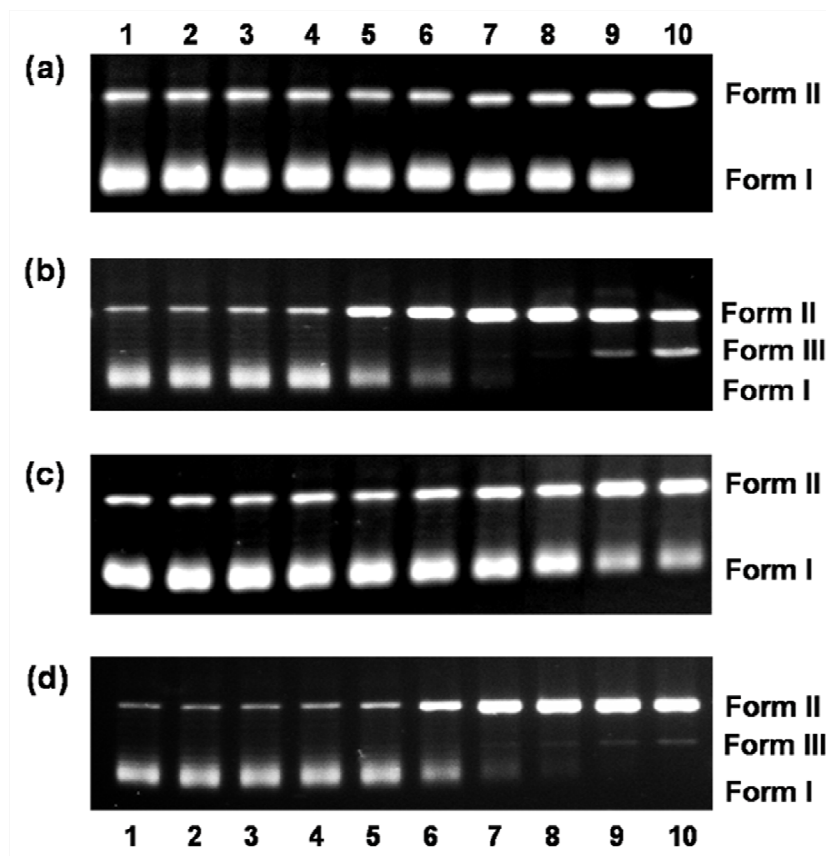
Fig. 8. Electrophoretic diagrams of supercoiled pBR322 DNA (0.2 μg, ~30 μM) cleaved by the complexes (a) $[Cu(L^1)(bipy)]Cl_2$ (**1**); (b) $[Cu(L^1)(phen)]Cl_2$ (**2**); (c) $[Cu(L^2)(bipy)Cl_2]$ (**3**) and (d) $[Cu(L^2)(phen)]Cl_2$ (**4**) in the presence of ascorbic acid (H_2ASC, 100 μM) in HEPES-buffer. Incubation at 37 °C for 1 h. Lane 1, plasmid DNA alone; lane 2, DNA + H_2ASC. For **1** and **3**; lanes 3−10, DNA + H_2ASC + [Complex] (10, 20, 40, 60, 80, 100, 200 and 400 μM, respectively). For **2** and **4**; lanes 3−10, DNA + H_2ASC + [Complex] (0.1, 0.2, 0.4, 0.6, 0.8, 1.0, 2.0 and 4.0 μM, respectively).
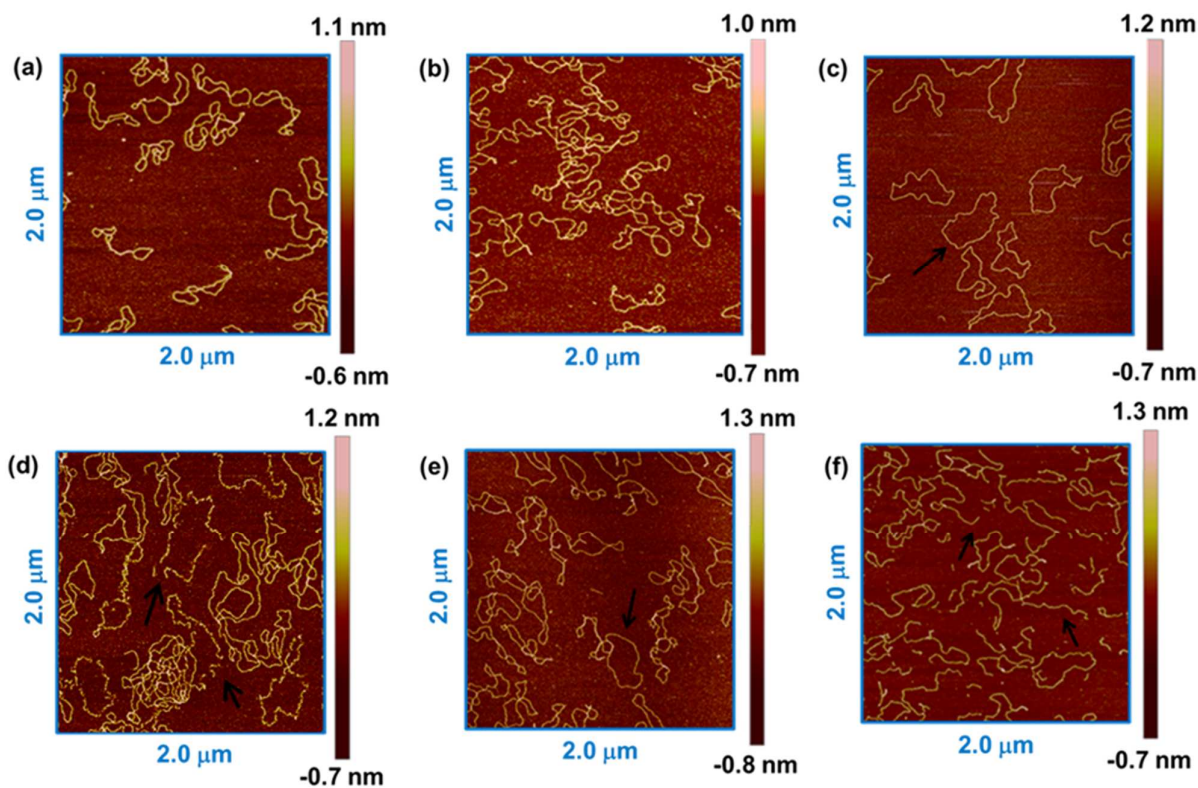
Fig. 9 AFM images showing the cleavage of supercoiled pBR322 DNA (0.2 μg) by the copper(II) complexes with ascorbic acid (H$_2$ASC, 100 μM) in HEPES-buffer. Incubation at 37 °C for 1 h. (a) DNA alone; (b) DNA + H$_2$ASC; (c) DNA + H$_2$ASC + **1** (400 μM); (d) DNA + H$_2$ASC + **2** (4.0 μM); (e) DNA + H$_2$ASC + **3** (400 μM) and (f) DNA + H$_2$ASC + **4** (4.0 μM). Arrows point the obtained DNA morphology after adding the copper(II) complexes and H$_2$ASC.

Tables

Table 1 ESI+ mass spectral data for **1-4**

Complex	m/z	Interpretation
$[Cu(L^1)(bipy)]Cl_2$ (**1**)	411	$[Cu(bipy)_2Cl+H]^{2+}$
	376	$[Cu(bipy)_2+H]^{2+}$
	335	$[Cu(L^1)(bipy)]^{2+}$
	322	$[Cu(bipy)Cl_2+H+CH_3OH]^+$
	173	$[L^1+Na+2H+CH_3OH]^{3+}$
	158	$[bipy+2H]^{2+}$
	151	$[L^1+3H+CH_3OH]^{3+}$
	119	$[L^1+3H]^{3+}$
$[Cu(L^1)(phen)]Cl_2$ (**2**)	458	$[Cu(phen)_2Cl]^+$
	424	$[Cu(phen)_2+H]^{2+}$
	403	$[Cu(L^1)(phen)+CO_2]^{2+}$
	359	$[Cu(L^1)(phen)]^{2+}$
	322	$[Cu(phen)Cl+CO_2]^+$
	182	$[phen+2H]^{2+}$
	173	$[L^1+Na+2H+CH_3OH]^{3+}$
$[Cu(L^2)(bipy)Cl_2]$ (**3**)	497	$[Cu(L^2)(bipy)Cl_2+2H]^{2+}$
	475	$[Cu(L^2)_2]^{2+}$
	449	$[Cu(bipy)_2Cl_2+4H]^{4+}$
	424	$[Cu(L^2)(bipy)–H]^+$
	400	$[Cu(bipy)_2+2H+Na]^{4+}$
	376	$[Cu(bipy)_2+H]^{2+}$
	208	$[L^2+2H]^{2+}$
	158	$[bipy+2H]^{2+}$
$[Cu(L^2)(phen)]Cl_2$ (**4**)	458	$[Cu(phen)_2Cl]^+$
	449	$[Cu(L^2)(phen)]^{2+}$
	424	$[Cu(phen)_2 + H]^{2+}$
	337	$[Cu(phen)Cl_2+Na+H]^{2+}$
	314	$[Cu(phen)Cl_2+H]^+$
	206	$[L^{2•}]^+$
	182	$[phen+2H]^{2+}$

3

Table 2 Electronic absorption and EPR spectral data of **1-4**

Complex	Electronic spectra, λ_{max}, $1/\lambda_{max}$ (nm, cm^{-1})						Spin Hamiltonian parameters			
	Solid	Appearance	MeOH	Appearance	DMSO	Appearance	$g_\parallel$	$g_\perp$	$A_\parallel$ (G)	A_N (G)
$[Cu(L^1)Cl_2]_2{}^a$	665, 15 049^b	light blue	680, 14 710	blue	674, 15 528	green	2.28	2.06	168	–
1	526, 19 029	purple	588, 17 123	purplish blue	572, 17 123 694, 14 409	green	2.18	2.04	203	14.8
2	533, 18 754	purple	585, 17 094	purplish blue	581, 17 212 704, 14 205	green	2.17	2.05	207	15.3
$[Cu(L^2)Cl_2]_2{}^a$	618, 16 175^b	deep blue	705, 14 180	blue	624, 16 025 936, 10 684	green	2.27	2.06	158	–
3	492, 20 300 560, 17 857	pink	525, 19 048	pink	489, 20 471	pink	2.15	2.05	216	17.6
4	567, 17 643	purple	587, 17 036	purplish blue	585, 17 094 697, 14 347	green	2.17	2.05	201	15.1

^{a} The starting complexes.

^{b} Data from reference.[16]

Table 3 Electronic absorption data of **1-4**, the starting compounds ($[Cu(L^1)Cl_2]_2$ and $[Cu(L^2)Cl_2]_2$) and other related copper(II) compounds upon

increasing amount of CT-DNA

Complex	Absorption, λ(nm)	Change in absorptivity^a	Shift (nm)	K_b (M^{-1})	References
Ethidium bromide (EB)	285	–	+ 1	5.52×10^6	This work
$[Cu(L^1)Cl_2]_2$	226	+	– 2	5.63×10^4	12
$[Cu(L^2)Cl_2]_2$	209	+	– 5	1.07×10^5	12
$[Cu(L^1)(bipy)]Cl_2$ (**1**)	302	–	+ 2	2.90×10^5	This work
$[Cu(L^1)(phen)]Cl_2$ (**2**)	204	–	+ 4	1.76×10^6	This work
$[Cu(L^2)(bipy)Cl_2]$ (**3**)	300	–	+ 1	1.44×10^5	This work
$[Cu(L^2)(phen)]Cl_2$ (**4**)	203	–	+ 1	8.77×10^5	This work
$[Cu(L^1)_2]Cl_2$	228	+	0	5.67×10^4	10
$[Cu(L^2)_2]Cl_2$	229	+	– 1	1.16×10^5	10
$[Cu(L^3)_2](ClO_4)_2 \cdot H_2O^b$	224	+	– 2	4.08×10^4	55
$[Cu(L^4)_2](ClO_4)_2 \cdot 2/3H_2O^c$	224	+	– 2	1.39×10^4	55
$[Cu(L^5)_2](ClO_4)_2 \cdot H_2O^d$	225	+	– 3	3.06×10^4	55
$[Cu(bipy)_2]^{2+}$	NR^e	NR^e	NR^e	3.24×10^4	56
$[Cu(phen)_2]^{2+}$	NR^e	NR^e	NR^e	2.75×10^3	57

^{a} + = hyperchromism; – = hypochromism. ^{b} L^3 = 1-amidino-*O*-2-methoxyethylurea. ^{c} L^4 = 1-amidino-*O*-2-ethoxyethylurea. ^{d} L^5 = 1-amidino-*O*-2-

buthoxyethylurea. ^{e} NR = not reported.

Table 4 Ellipticity (mdeg) and wavelengths (nm) for the interactions of CT DNA (200 μM) with the copper(II) complexes

Complex	[Complex]/[DNA]	Positive band				Negative band			
		λ_{max}	$\Delta\lambda_{max}$	θ_{max}	$\Delta\theta_{max}$	λ_{min}	$\Delta\lambda_{min}$	θ_{min}	$\Delta\theta_{min}$
DNA		275		15.86		245		−18.82	
Ethidium bromide	0.5	273	− 2	24.64	+8.78	247	+2	−35.57	+16.75
	1.0	272	− 3	41.94	+26.08	247	+2	−61.51	+42.69
[Cu(L^1)(bipy)]Cl$_2$ (**1**)	0.5	277	+ 2	14.65	−1.21	246	+1	−17.25	−1.57
	1.0	276	+ 1	14.88	−0.98	245	0	−12.76	−6.06
[Cu(L^1)(phen)]Cl$_2$ (**2**)	0.5	279	+ 4	33.77	+17.91	249	+4	−14.84	−3.98
	1.0	281	+ 6	36.88	+21.02	250	+5	−12.79	−6.03
[Cu(L^2)(bipy)Cl$_2$] (**3**)	0.5	280	+ 5	13.54	−2.32	246	+1	−18.20	−0.62
	1.0	279	+ 4	12.95	−2.91	246	+1	−17.86	−0.96
[Cu(L^2)(phen)]Cl$_2$(**4**)	0.5	279	+ 4	30.05	+14.19	248	+3	−16.68	−2.14
	1.0	281	+ 6	34.58	+18.72	249	+4	−15.81	−3.01

1 **Table 5** Melting temperature of CT DNA in the presence of the complexes at different

2 [Complex]/[DNA] ratios

[Complex]/[DNA]	T_m (°C)				ΔT_m (°C)^a			
	1	**2**	**3**	**4**	**1**	**2**	**3**	**4**
0.5	81.9	82.1	81.5	81.7	+0.8	+1.0	+0.4	+0.6
1.0	82.2	84.0	82.1	83.4	+1.1	+2.9	+1.0	+1.3
1.5	82.6	84.6	82.8	84.4	+1.5	+3.5	+1.7	+3.3
2.0	84.3	87.5	83.2	84.7	+3.2	+6.4	+2.1	+3.6

3 ^{a} T_m of CT DNA = 81.1 °C.

4 **Table 6** Anticancer activities of **1-4** and the related compounds towards three human cancer cell lines
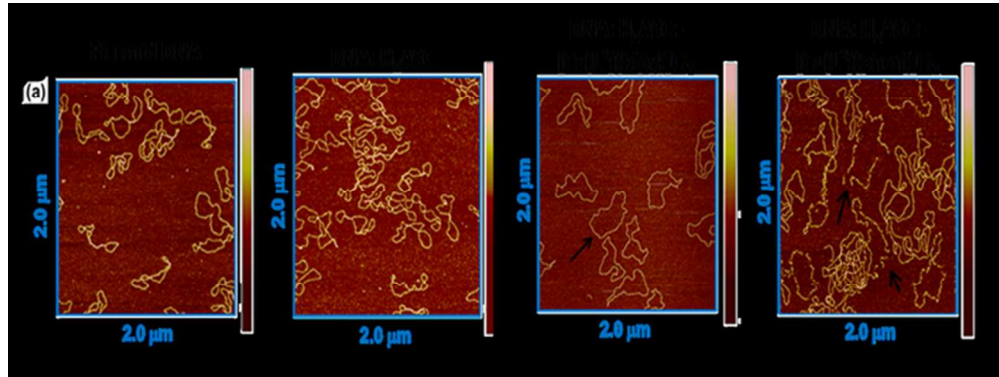
Complex	IC$_{50}$ (µg mL^{-1})		
	KB	MCF-7	NCI-H187
$[Cu(L^1)Cl_2]_2{}^a$	Inactive	Inactive	49.42
$[Cu(L^2)Cl_2]_2{}^a$	22.51	Inactive	47.63
$[Cu(L^1)(bipy)]Cl_2$ (**1**)	17.97	6.61	24.23
$[Cu(L^1)(phen)]Cl_2$ (**2**)	1.08	0.97	1.07
$[Cu(L^2)(bipy)Cl_2]$ (**3**)	Inactive	Inactive	39.53
$[Cu(L^2)(phen)]Cl_2$ (**4**)	5.10	3.00	5.01
2,2′-bipyridine	Inactive	Inactive	13.16
1,10-phenanthroline	28.50	40.04	7.93
Cisplatin	27.01	Inactive	Inactive

5 ^{a} The starting complexes.

6 **Table 7** Antibacterial activities of the complexes **1-4** and enrofloxacin against three human food-

7 poisoning bacteria

Complex	MIC (mg mL^{-1})		
	E. coli	*Salmonella*	*Campylobacter*
$[Cu(L^1)Cl_2]_2{}^a$	25.00	25.00	3.12
$[Cu(L^2)Cl_2]_2{}^a$	25.00	12.50	3.12
$[Cu(L^1)(bipy)]Cl_2$(**1**)	–	–	0.25
Cu(L^1)(phen)]Cl$_2$ (**2**)	1.00	0.25	0.063
$[Cu(L^2)(bipy)Cl_2]$ (**3**)	–	–	–
$[Cu(L^2)(phen)]Cl_2$ (**4**)	1.00	1.00	0.125
Enrofloxacin	0.008	0.002	0.015

8 ^{a} The starting complexes.

29x11mm (600 x 600 DPI)